ASSESSING THE ACUTE TOXICITY OF PHOTODEGRADED ANTHRACENE WITH IN VITRO AND IN VIVO SKIN MODELS

A Thesis

by

MOLLY BRZEZINSKI

BS, Arizona State University, 2017

Submitted in Partial Fulfillment of the Requirements for the Degree of

MASTER OF SCIENCE

in

MARINE BIOLOGY

Texas A&M University-Corpus Christi
Corpus Christi, TX

August 2022

August 2022

ASSESSING THE ACUTE TOXICITY OF PHOTODEGRADED POLYCYCLIC AROMATIC HYDROCARBONS WITH IN VITRO AND IN VIVO SKIN MODELS

A Thesis

by

MOLLY BRZEZINSKI

This thesis meets the standards for scope and quality of
Texas A&M University-Corpus Christi and is hereby approved.

Wei Xu, PhD
Chair

Frauke Seemann, PhD
Committee Member

Jeremy Conkle, PhD
Committee Member

Lin Zhu, PhD
Committee Member

August 2022

ABSTRACT

The Gulf Coast of Texas is heavily inundated with petroleum refineries that release Polycyclic Aromatic Hydrocarbons (PAHs) into nearby waters, and these chemicals may pose a threat to human health when they interact with environmental conditions. PAHs are a group of hundreds of different chemicals, and the Environmental Protection Agency has identified 16 priority PAHs. Many of these chemicals are acute skin irritants and can cause skin, lung, bladder, and liver cancer with chronic exposure. Humans can be exposed when they interact with contaminated air, soil, and water. Recent studies have demonstrated that abiotic factors such as UV light, salinity, and pH can modify PAH structure, however, it is unknown how these modifications affect acute toxicity to the human skin barrier.

The objectives of this study were to characterize the phototoxic effects of a priority PAH, anthracene by testing photodegradation treatments on cell culture and animal models. Gas chromatography and mass-spectroscopy confirmed the presence of 1,9-anthraquinone and phthalic acid, both known skin irritants, in photodegradation products. Keratinocyte cell culture was used to assess the impacts of photodegraded anthracene on cell migration, viability, and stratification development. We found that longer photodegradation times resulted in decreased cell viability and increased migration. A unique three-dimensional stratification assay demonstrated that photodegraded anthracene reduces differentiation in apical keratinocytes. Relative gene expression analysis suggests that keratinocytes bypass *TLR-4* activation and utilize *IL-1α, IL-1β,* and *TNF-α* to produce an inflammatory response. *Mus musculus* studies indicate that extracellular matrix remodeling may be induced by 4, 8, and 24-hour photodegraded intermediates by keratinocyte-derived *Il-1β, S100a9, Mmp1*, and *Connexin43*. The results of this study indicate that photodegradation can produce intermediates that may elicit dermal

inflammation, and the presence of these intermediates should be evaluated in bays with high foot-traffic.

ACKNOWLEDGEMENTS

I would like to thank my committee chair, Dr. Wei Xu for his dedication to instructing me in cell culture and entertaining my many scientific questions. I am thankful to have grown into a critically thinking scientist under his direction. I would also like to thank my committee members Dr. Frauke Seemann, Dr. Jeremy Conkle, and Dr. Lin Zhu for pushing me to question my research approaches and interpretations. I have so much appreciation for the members of the Xu lab who have helped me in all things from data collection and revising manuscripts to lending an ear when I needed it most: Dr. Leisha Martin, Sandra Marbach, Chi Huang, Kayla Simpson, Kenzie Merrill, and Nin Gan. Thank you also to the incredible undergraduate students Kaitlin Garcia and Carly Armedarez for their willingness to be mentored and their stalwart attitudes.

Lastly, I would like to acknowledge the Texas Sea Grant Grants-in-aid of Graduate Research and the National Institute of Environmental Health Sciences for funding this research and supporting the health of our coastal ecosystems.

TABLE OF CONTENTS

Page

LIST OF FIGURES

Page

LIST OF TABLES

Page

1. INTRODUCTION

Background and Relevance

Polycyclic Aromatic Hydrocarbons

PAHs are formed from incomplete combustion reactions, and can be petrogenic and pyrogenic (US Environmental Protection Agency, 2013). They are typically released into the environment through wildfires, oil spills and refinery activity, and automobile exhaust. The Gulf Coast of Texas is heavily inundated with petroleum industries that release a sustained amount of PAHs into the surrounding air, soil, and water (Rowe et al., 2020). Recent assessments by the Coastal Bend Bays and Estuaries Program found total PAH concentrations in Nueces Bay at 2653.3 ng/g soil for some sites (Abdulla & Murgulet, 2021). For reference, areas with a total PAH abundance greater than 1000 ng/g soil are considered heavily polluted, and weak pollution is considered for sites with PAH concentrations between 200-600 ng/g soil (Patel et al., 2020).

The unique chemical structure of PAHs affects their persistence in soil, suspended sediment, and water (Lu et al., 2011; Lyszczarz, 2021). Molecular weight is an influential characteristic and can affect the solubility, bioavailability, and retention time of a PAH in the environment (Abdel-Shafy et al., 2016). PAHs with less than four aromatic rings are classified as lower molecular weight and those with more than four are classified as high molecular weight (Jameson, 2019). Higher molecular weight PAHs in their parent form may persist in the environment longer than lower molecular weight counterparts, and their stronger affinity to sediment makes them less bioavailable (Abdel-Shafy et al., 2016). In contrast, lower molecular weight PAHs are more likely to remain in the water column where they can interact with abiotic factors, such as UV light, pH, and salinity, in addition to biota (Abdel-Shafy et al., 2016). Unfortunately, these particular compounds are also the most cited for their range of toxic effects,

and studies with zebrafish models confirm that oxygenated, hydroxylated, or nitrated PAH derivatives are generally more toxic than parent PAH compounds (Geier et al., 2018).

Humans can be exposed to PAHs in the environment through contaminated air, soil, and water, and several factors increase the risk of dermal exposure to PAHs. The retention time for PAHs in tidal flats and bay systems can be as much as 20 years, and both PAHs and their intermediates can persist in the environment although there is less information about how long intermediates may remain (Hoffman et al., 2003; Marquès et al., 2016). Additionally, the contaminated deposits can be re-agitated by currents, heavy ship traffic, and dredging which is common in the bay systems in and around Corpus Christi (Bacosa et al., 2017). These factors increase the risk of dermal exposure to PAHs and PAH intermediates in turbid waters that are typical in coastal estuaries.

Two and three-ring PAH compounds are common composites in weathered petroleum and are more likely to persist in the environment by cycling through episodes of volatilization and deposition (Hayakawa et al., 2006). The present study focuses on a priority two-ring PAH, anthracene. Anthracene has a relatively high solubility in water compared to other priority PAHs and is soluble in water at 0.29 ppm at 50^{o}C (Blumer & Youngblood, 1975). Anthracene was selected as a study chemical based on the known abundance in the Texas Coastal Bend bay system and its potent toxicity (Abdel-Shafy et al., 2016; Abdulla & Murgulet, 2021; Gamble et al., 1989; IPCS, 1998; Liu et al., 2011).

PAH Toxicity and Phototoxicity

PAHs in their parent forms are known to cause several types of cancer depending on exposure routes (CDC, 2013; Stec et al., 2018). The International Agency for Research on Cancer found that skin, lung, bladder, liver, and stomach cancers are associated with long-term

exposure in occupational settings (IARC, 2010). At present, there is agreement among the U.S. Department of Health and Human Services (HHS), International Agency for Research on Cancer (IARC), and US Environmental Protection Agency that benzo(a)pyrene and benzo(a)anthracene are at least a probable carcinogen (CDC, 2013).

Several PAHs cause acute skin irritation and repeated exposure to irritants can initiate chronic inflammatory skin diseases like psoriasis and atopic dermatitis in individuals with genetic predispositions (Pasparakis et al., 2014; IPCS, 1998). Previous studies have characterized PAHs and their metabolites as primary irritants to the skin, although pathway analysis remains unclear (Sowada et al., 2017). Anthracene is a skin irritant and has been shown to increase dermal sensitivity to UV light after pre-exposure to treatments (IPCS, 1998). Melanocytes that are continuously treated with PAHs and UV are likely to develop skin carcinogenesis (Baudouin et al., 2002). Because a primary irritant can initiate chronic skin inflammation in genetically vulnerable individuals, it is important to understand the extent and mechanisms of acute irritation to better predict the risk of skin disease development in exposed populations.

Phototoxicity describes the phenomena by which the toxicity of a compound is enhanced by UV exposure via alteration of the chemical structure. In PAHs, UV light had been shown to induce excited states, which can react with oxygen and other excited-state PAHs to produce reactive oxygen species (ROS), endoperoxides, and quinones (Fu et al., 2012; Yu et al., 2002). Benzo(a)pyrene, a 5-ring PAH, can produce at least three structurally unique quinones after UV irradiation (Yu et al., 2002).

The majority of current research on PAH phototoxicity focuses on the risk to aquatic life, of which bivalves and gastropods in their larval and juvenile life stage are commonly cited (Honda et al., 2020; Geier et al., 2018; Pelletier et al., 2009). Additional studies on microbial life

have demonstrated phototoxic and photomutagenic effects of PAHs in bacterial species with concurrent PAH and UV light exposure (Yan et al., 2004). Limited studies on the phototoxicity of PAHs to keratinocyte cell lines suggest that two and three-ring PAHs are not phototoxic with the exception of anthracene (Wang et al., 2007). Four-ring PAHs exhibited the greatest phototoxicity at increasing concentrations when evaluated by cell viability assays (Wang et al., 2007). However, these studies only took a single degradation timepoint into consideration, and more research is necessary to fully understand how the toxicity of photodegraded PAHs changes with degradation time.

Approaches to laboratory PAH photodegradation vary widely with regard to the light source, wavelength, solar irradiance, and initial concentration (Behymer & Hites, 1985; Fasnacht & Blough, 2002; Kim et al., 2013). Due to these variations in experimental conditions, the calculated half-life of anthracene varies greatly from approximately 12 minutes to two hours (National Center for Biotechnology Information, 2021; Huang et al., 1995, Seopela et al., 2021). Fewer studies have looked at the production of photodegradation compounds, and half-life does not necessarily correlate with the presence of a single degradation compound. Despite inconsistencies in the literature, degradation kinetics are pseudo-first-order and there is consensus that PAHs absorb light in the 300-420nm range (Huang et al., 1995). In the present study, anthracene was degraded under the visible spectra ranging from 300 to 800nm with subsampling performed at 0, 1, 4, 8, and 24 hour time points to ensure spectral overlap that will include effects from the parent compound and production of intermediates.

Epidermal Structure and Dermatitis

The skin barrier is our first line of defense against a variety of environmental stressors and chemicals. Anthracene is a known skin irritant and its absorbance within the visible light

range makes it an ideal candidate for phototoxicity studies (Rengarajan, 2015). To understand exposure risk, the toxicity of anthracene and its photodegraded products were assessed using *in vitro* human skin cell models. The human skin is comprised of the epidermis and the dermis. The epidermis is a multilayer epithelium made up of keratinocyte cells and the dermis contains fibroblasts and other stromal cells embedded in an extracellular matrix (Yousef et al., 2021). The epidermis is constructed of five distinct sublayers that extend from the basement membrane, including the stratum basale, stratum spinosum, stratum granulosum, stratum lucidum, and the stratum corneum from the basal to apical layers of the epidermis. The stratum basale consists of a single layer of basal keratinocyte cells that divide and facilitate the replacement of cells in the superficial layers. Differentiated cells move upward from the stratum basale into the stratum spinosum where they adhere to their neighboring cells through tight junctions and desmosomes create a water-tight barrier. Damage to these cell-cell connections can negatively impact the water homeostasis of the epidermis (Natsuga, 2014).

In addition to cell-cell connections, a functioning skin barrier requires robust structures within keratinocytes. Cytokeratins are a group of intracellular keratin proteins that support the internal structure of keratinocytes. Keratinocytes express different cytokeratins throughout their development, and their presence or absence signifies the degree of cell differentiation in the mature epidermis (Rosso et al., 2016). Cytokeratin 14 is constitutively expressed in basal cells, and cytokeratin 10 is enriched in terminally differentiated cells in suprabasal layers. These cytokeratins are ideal markers for keratinocyte differentiation, which can be used as an indicator of epidermal development (Guo et al., 2020; Zhang, 2018). Changes in the expression of these proteins can suggest an altered stratification state which impacts skin barrier function. For example, mutations in the genes responsible for cytokeratin 14 produce the skin blistering and

basal keratinocyte lysis phenotypes typical of epidermolysis bullosa simplex (EBS) (Guo et. al., 2020). The remaining three layers include the stratum granulosum, stratum lucidum, and stratum corneum, which constitute the progressive development of keratinocytes to highly keratinized cells.

Although keratinocytes are the most abundant cell type of the epidermis, this epithelial layer also includes several other cell types (Yousef et al., 2021). Melanocytes are scattered along with the basal cells and are responsible for pigmentation. Merkel cells are used to sense pressure throughout the epidermis, and they connect to sensory nerves in the dermis. Langerhans cells are resident macrophages that bridge the innate and adaptive immune systems (Clayton et al., 2017). They are phagocytotic cells that sample the epidermal environment and can migrate to lymph nodes to activate the adaptive immune response (West & Bennett, 2018). Importantly, Langerhans cells can be stimulated by keratinocytes, and this communication between structural and immune cells is vital to the host defense against stressors and pathogens (Clayton et al., 2017; West & Bennett, 2018).

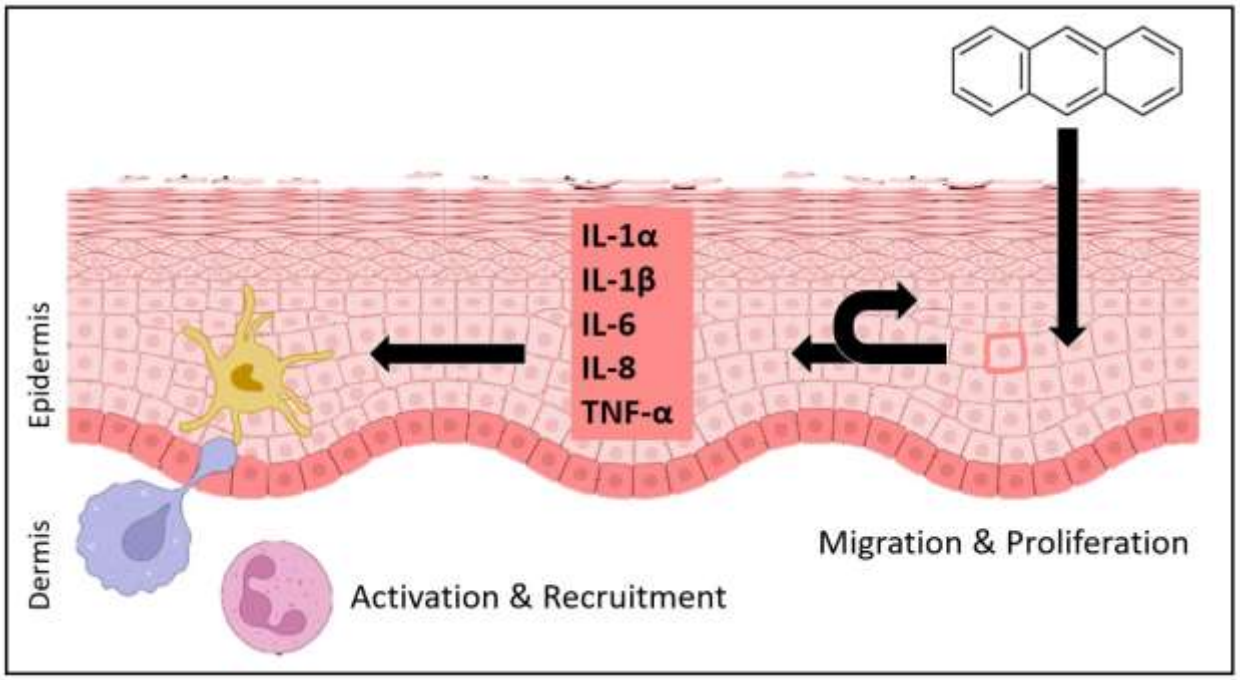

Figure 1: Initiation and response of epidermal tissure to keratinocyte-derived proinflammatory cytokines under chemical exposure (Slodownik, 2008; Bains, 2018). Image created on biorender.com.

Keratinocytes in the epidermis are the first cells to respond to environmental stressors and subsequently initiate different kinds of dermatitis depending on genetic predispositions and the duration and intensity of the contact (Bains, 2018). Irritant contact dermatitis describes the acute response of keratinocytes to external stressors such as UV light, pathogens, physical irritants, and chemicals (Bains, 2018). The irritant is thought to damage apical keratinocytes and impair the epithelial barrier, which stimulates the release of cytokines, such as Interleukin 1α (*IL-1α*), Interleukin 1β (*IL-1β*), Interleukin 6 (*IL-6*), Interleukin 8 (*IL-8*), and tumor necrosis factor α (*TNF-α*) by neighboring keratinocytes (Slodownik, 2008; Bains, 2018) (Figure 1). These cytokines can stimulate Langerhans cells and recruit other innate immune effector cells like non-tissue resident macrophages and neutrophils (Leonard & Guttman-Yassky, 2018). Keratinocytes can respond by migrating, proliferating, and differentiating. This process can cause further skin

barrier impairments that lead to host skin transepidermal water loss (TEWL) and susceptibility to environmental stressors (Ronfard & Barrandon, 2001).

Purpose, Objectives, and Hypothesis

The purpose of this study is to evaluate the phototoxic and epidermal developmental effects of the photodegraded anthracene using a HaCaT keratinocyte cell model and SKH1-Elite hairless *Mus musculus* animal model. Direct cytotoxicity to keratinocytes can predispose skin to irritant contact dermatitis, and surviving keratinocytes respond to exogenous stressors by migrating and proliferating. Chemicals that are absorbed by the skin may cause basal cells to alter the differentiation of apical epidermal layers through changes in proliferation and cytokeratin expression (van den Bogaard et al., 2015; Alalaiwe et. al., 2020). These changes can lead to impaired epidermal development that inhibits the function of the stratum spinosum to maintain a water-tight barrier against environmental exposures.

These key cellular responses can be precisely modeled with two-dimensional monolayer cell culture and by constructing three-dimensional stratification models with an established method (Xu et al., 2018). Cell migration is typically modeled *in vitro* by measuring the re-adherence of nonproliferating cells after an abrasion is made through a confluent two-dimensional culture (Liang et al., 2007). Advances in the dermatoxicity field have yielded more representative cell models made up of stratified keratinocytes grown in three-dimension (Gotz et al., 2012; Zanoni et al., 2014). Daily exposure to a chemical during stratification development creates an ideal model to assess the effects of repetitive exposure on skin development, with implications for skin barrier integrity.

These functional assays will be corroborated with genetic analysis to understand the putative pathway for phototoxicity. By focusing on a broad range of genes in a distinct cell

population like keratinocytes, we can identify the specific cellular responses that initiate inflammation and signal immune cell recruitment. This represents the first step in understanding how to prevent inflammation in environmental exposures and is advantageous to the development of targeted therapeutics that can intercept the inflammatory response at the receptor level.

However, the main limitation of cell culture methods for skin studies is the lack of immune recruitment and cross-talk between keratinocytes and inflammatory cells. *In vitro* studies allow for immune involvement and provide evidence to support a molecular mechanism of acute PAH phototoxicity. The SKH1-Elite mice are commonly used for chemical dermatoxicity and photoexposure studies due to their hairless phenotype and immunocompetence (Avci et al., 2013). This strain demonstrates pronounced similarities in skin organization and carcinogenic response to UVR in addition to cutaneous responses (Benavides et al., 2009). The SKH1-Elite model is ideal to visualize skin irritation and model the human epidermis. Differential gene expression of isolated keratinocytes after treatment exposures with *in vitro* models allows us to measure the initiation of irritant contact dermatitis, in which keratinocytes then direct the subsequent recruitment and assembly of additional innate and adaptive cells. Repetitive exposure to skin irritants increases the risk of atopic dermatitis, which is a chronic, internally-mediated inflammatory condition that may persist in the absence of the initial chemical stressors (Bains, 2018). Pathway analysis of keratinocyte-derived proinflammatory signals can suggest if repetitive acute exposures can lead to these chronic conditions. However, the use of human keratinocytes in cell culture may provide more representative effects of photodegraded anthracene in humans because of the exact similarity of genetic makeup. By

using both HaCaT keratinocyte cell-based methods and a murine model approach, we were successful in understanding the putative keratinocyte inflammation pathway in humans.

Our objectives were to 1) Assess the effects of photodegraded anthracene on keratinocyte migration, cell viability, and epidermal stratification. 2) Investigate the epidermal effects of topical photodegraded anthracene exposure using histological methods and keratinocyte gene expression analysis. It was hypothesized that photodegraded anthracene intermediates would modify superficial wound-healing capabilities and skin barrier integrity, and alter epidermal development as exemplified by changes to cell migration, viability, and epidermal stratification patterns. These effects are expected to be reflected in the mouse model as changes in epidermal thickness and differentially expressed inflammatory genes.

2. METHODS AND MATERIALS

Chemical Analysis with GC-MS

Analysis of the photodegraded samples was performed using Gas-Chromatography Mass-Spectrometry (Thermo Scientific TSQ 9000 EVO Triple Quadrupole GC-MS/MS, 28 m, 0.25 mm, 0.25 μm capillary column). Mass spectrometry was acquired using the electron ionization (EI) and selective reaction monitoring (SRM) modes. First, a serial dilution of the anthracene analytical standard in acetone was prepared and injected at 280ºC in splitless mode with a transfer line and ion source temperature of 300ºC and 320ºC respectively. The beginning column temperature was held at 80°C for 1 minute, then raised to 330°C at the rate of 30°C/minute, and held at the final temperature for 5 minutes. Helium was used as a carrier gas at a constant flow rate of 1.2 mL/minute. The resulting values were used to construct a standard curve and equation. Stock solutions of anthracene were photodegraded for 1, 4, 8, and 24 hours and analyzed according to the same procedure to quantify the amount of anthracene remaining in the photodegraded solutions. Concentrations of anthracene in photodegraded samples were back-calculated based on the standard curve equation.

An untargeted analysis of photodegraded samples was performed using Gas-Chromatography and Mass-Spectroscopy (Shimadzu GC-MS QP2020 NX 30 m, 0.25 mm, 0.25 μm capillary column) to characterize photodegraded products. Samples were injected at 250°C in split mode with an ion source an interface temperature of 250°C. The beginning column temperature was held at 40°C for 1 minute, then raised to 240°C, 280°C, and 320°C at a rate of 10°C/minute, 4°C/minute, and 10°C/minute. Helium was used as a carrier gas at a rate of 2 mL/minute. Species were indentified by comparison with a NIST database.

Cellular Studies

Cell culture

A human keratinocyte cell line (HaCaT) was grown under sterile conditions to 90% confluence in Keratinocyte Serum-Free Medium (Gibco) with Keratinocyte Growth Supplement (Gibco) and 1% Streptomycin/Penicillin (Hyclone) at 37°C and 5% CO_2. Cells used for MTT assays were continued in this keratinocyte media whereas cells used in migration assays were passed with Dulbecco's Modification of Eagle's Medium (DMEM) (with 4.5g/L L-glutamine & Sodium Pyruvate, Corning) and 10% heat-treated Fetal Bovine Serum (100% US Origin, SeraDigm), and 1% Streptomycin/Penicillin (Hyclone) and grown to 90% confluency. Cells used in gene expression studies were plated in the same media as the migration studies without the Fetal Bovine Serum. Three-dimensional assay cells were stratified in a house-made E-media (Table 1).

Table 1: Table of reagents for E-media used to induce stratification in three-dimensional assay

Reagent	**Volume**
Dulbecco's Modification of Eagle's Medium (Corning)	50:50 (v/v)
Dulbecco's Modification of Eagle's Medium-F12 (Corning)	50:50 (v/v)
Adenine	18 μM
Bovine Pancreatic Insulin	500 ng/mL
Human Apo-transferring	500 ng/mL
triiodothyronine	500 ng/mL
L-glutamine	4mM
Hydrocortisone	0.4 μg/mL
Cholera Toxin	10 ng/mL
Recombinant Human Epithelial Growth Factor (EGF)	5 ng/mL
Fetal Bovine Serum (FBS)	5% (v/v)

Preparation of photodegraded anthracene

Anthracene solutions in water were prepared by a preliminary dilution in ethanol (Fischer Scientific). The final solution constituted less than 0.1% ethanol in water. Anthracene was photodegraded using the Suntest CPS+ solar simulator chamber (Atlas) at 1 ppm in mili-Q water.

Each hour of irradiation is approximately equivalent to 1.2 h of direct sunlight at 30°N latitude during the June solstice, and the range for irradiance is 300-800nm. Sub-samples were taken at 0, 1, 4, 8, and 24 hour timepoints and stored in sterile borosilicate vials with tinfoil and parafilm seals and stored at 4^{o}C. Samples were filtered with a 0.22 μm cellulose acetate membrane filter (VWR) prior to dilution with media for cell application.

Migration Assay

HaCaT keratinocytes were grown to 90% confluency and passed in Dulbecco's Modification of Eagle's Medium (4.5 g/L L-glutamine & Sodium Pyruvate, Corning) with 10% heat-treated Fetal Bovine Serum (100% US Origin, SeraDigm), and 1% Streptomycin/Penicillin (Hyclone) (DMEM++) to 90% confluency. Cells were seeded in a 12-well plate (VWR Tissue Culture Plate, Surface treated, Sterile) at 100,000 cells per well and grown overnight to ensure a uniform monolayer. Each well represents a single replicate, and 6 replicates were perfomed for each treatment. Wells were then treated with 0.5 mg/mL Mitomycin in DMEM++, for 4 hours and washed twice with DPBS (Dulbecco's Phosphate Buffered Saline, Lonza BioWhittaker). A single vertical scratch was made with a 10XL pipette tip (Biotix) and wells were washed with DPBS to remove excess cellular debris. Three images per well were taken of the initial scratch with a 20x objective. Each well was treated for 24 hours with photodegraded anthracene diluted to 0.10 ppm, 0.02 ppm, or 0.005 ppm in DMEM++ or media only for control samples. Scratches were re-imaged at the same location after 24 hours and measured with the arial lasso function in ImageJ. Following equation:

$$percent\ gap\ closure = \frac{(initial\ gap\ area_{avg} - final\ gap\ area_{avg})}{initial\ gap\ area_{avg}}$$

This procedure was performed with two trials for a total of 6 replicates per treatment dilution. All percent gap closure values were normalized to the control gap values for their

respective trials and pooled after normalization. A one-way ANOVA was run with Tukey *post hoc* tests in R Studio to assess significance between treatments.

Cytotoxicity Assay

An MTT Assay was performed according to the manufacturer's instructions (Sigma Aldrich). HaCaTs grown to 90% confluency in Keratinocyte Serum-Free Medium (Gibco) with Keratinocyte Growth Supplement (Gibco) and 1% Streptomycin/Penicillin (Hyclone) (KSFM++) were seeded at 100,000 cells per well in a 96 well-plate (VWR). A single well was considered a replicate, and 6 replicates were performed for each treatment. Cells were grown overnight and treated with 0.10 ppm 0.02 ppm, and 0.005 ppm dilutions of photodegraded anthracene in KSFM++ with 6 replicates per dilution per treatment. KSFM++ only was used as a control, and blanks without cells were performed to subtract background absorbance of MTT reagents. Treatment media was removed after an 18 hour exposure and 50uL KSFM++ with 50uL MTT was added to each well per the manufacturer's instructions. After a 3 hour incubation at 37^{o}C, 150 μL MTT solvent was added to each well and the plate was gently agitated on a shaker-plate at room temperature (VWR Incubating Mini Shaker) for 15 minutes. Absorbance at OD=590nm was read by Cytation 5 Image Reader (BioTek). Background absorbance was subtracted from all treatment and control wells, and control replicates were averaged. Percent viability was calculated by dividing treatment OD values by the average of controls. A one-way ANOVA was run with Tukey *post hoc* tests in R to assess significance between treatment group viability.

Three-Dimensional Stratification Assay

HaCaT keratinocytes were grown in DMEM++ and seeded at 500,000 cells per well in 0.4 μm mesh 12-well insert plate (Corning). 1.0 mL of DMEM++ was added to the bottom of each insert, and 0.5mL remained above the insert. Cells were allowed to adhere for 24 hours

before daily treatments began and each well was considered a replicate. Wells were treated daily with 0.5mL of 0.10 ppm photodegraded anthracene in house-made E-Media with a total of 4 replicates per treatment. Media was applied to the bottom of the well-insert for 8 hours and then replaced with fresh media for 16 hours. After 14 days of stratification, inserts were washed three times with DPBS and stored in 4% paraformaldehyde at 4^{o}C for histological processing.

Mesh inserts were manually cut out of their frame with a sterile razor and placed into histological cassettes with filter paper and a sponge (SPL Life Sciences). Cassettes were fixed in 10% neutral buffered formalin (Thermo Scientific) for 24 hours and processed according to a 14-hour human tissue protocol in Excelsior AS Tissue Processor (Thermo Scientific) (Table 2).

Table 2: 14-hour human tissue processing protocol with dehydration, infiltration, and clearing steps.

Reagent	**Time (hours)**
50% Ethanol	2:00
70% Ethanol	1:00
95% Ethanol	0:30
95% Ethanol	0:30
100% Ethanol	1:30
100% Ethanol	1:30
100% Ethanol	1:00
100% Xylene	1:00
100% Xylene	1:00
Paraffin Wax	1:00
Paraffin Wax	2:00
Paraffin Wax	1:00

Samples were embedded in paraffin using a Histostar (Thermo Scientific), and cross-sections were stained with Hemotoxylin (VWR) and Eosin (VWR) according to a standard protocol and mounted with Permount solution (Fisher Chemical) and glass coverslips (St. Michael's Hospital Research).

Three images were taken of each cross-section with a 20x objective and analyzed in ImageJ. Briefly, the average height of epithelia was calculated by measuring the total sample

area and dividing this by the length of the sample. ImageJ scale was appropriately set using a micro-ruler. An ANOVA with Tukey *post hoc* test was used to calculate significant differences in epithelial thickness across treatments and control.

An additional set of 5 µm slides were stained for cytokeratin 10 and DAPI according to a standard protocol (Wang et al., 2016). Briefly, cross-sectional slides were deparaffinized and rehydrated according to the same procedure for H&E staining. Heat-induced epitope retrieval was performed using a citric acid buffer solution (housemade) and samples were washed three times in DPBS (Lonza BioWhittaker) before a 10% Lamb blocker incubation at room temperature for 1 hour. Samples were washed and incubated overnight at 4^{o}C with anti-human Cytokeratin 10 or 14 Antibody (Miltenyi Biotec) and later incubated with a compatible Alexa Fluor Antibody before a final stain with DAPI (0.25 mg/mL). Slides were mounted with ClearMount solution (Invitrogen) and glass coverslips and imaged immediately with an upright microscope. Fluorescent images were taken with red, green, and DAPI filters and later merged. Exposure time was consistent for each image and sample.

Quantification of Gene Expression with RT-qPCR

HaCaT keratinocytes were grown for no more than five passes in KSFM++ and plated at 500,000 cells per well in a 6-well plate (Corning) in DMEM++. Cells were allowed to adhere to the plate before media was replaced with Dulbecco's Modification of Eagle's Medium with 4.5 g/L L-glutamine & Sodium Pyruvate (Corning) and 1% Streptomycin/Penicillin (Hyclone) (DMEM+). Each well was considered as a replicate and 2 trials of 3 replicates per treatment were performed for a total of 6 replicates per treatment. Photodegraded anthracene was diluted 10 times in DMEM+ and applied to cells for 4 and 16 hours. After treatment, cells were washed

three times in DPBS (Lonza BioWhittaker) and collected with 500 µL Trizol Reagent (Ambion by Life Technologies) and stored at -80 ºC.

RNA extraction was performed according to a standard protocol with RNA-free reagents. Briefly 200 µL of chloroform was added to each 2mL RNA tube and shaken to separate salts from solution. After a 5 minute incubation at room temperature, each tube was centrifuged for 20 minutes at 12,000 rpm at 4ºC. 400 µL of the colorless supernatant was transferred to a new 1.5 mL tube and 400 µL isopropanol was added to precipitate out RNA and DNA. After an overnight incubation at -20ºC, samples were centrifuged for 20 minutes at 12,000 rpm (4ºC) and supernatant was discarded. The pellet was rinsed with 1.0 mL of 70% ethanol prepared with RNA-free water and then air-dried at room temperature. The resulting pellet was dissolved in a master mix prepared according to table 1 for 30 minutes at 37ºC and inactivated with 5 µL DNase removal agent (Invitrogen). Samples were centrifuged for 8000 g for 5 minutes before 25 µL of supernatant was collected and stored in a new 1.5 mL Eppendorf tube and stored at -80ºC.

The quantity and quality of extracted samples was determined by A260/280 and A260/230 values as assessed by Eppendorf Biospectrometer. Appropriate dilutions were made for RNA samples over 500 ng/µL and cDNA was synthesized according to an in-house protocol with Oligo dT random hexamer (IDT) using MiniAmp Plus Thermal Cycler (Thermo Fisher Scientific). Briefly, 0.5 µL dNTP and 0.5 µL Oligo dT random hexamer (IDT) were added to 5.5 µL of RNA in PCR tubes. Samples were processed in the MiniAmp Plus Thermal Cycler for the first 2 steps of a program that consisted of 5 minutes at 65 ºC, 10 minutes at 4 ºC, 10 minutes at 23 ºC , 20 minutes at ºC , and 10 minutes at 80 ºC before an indefinite hold at 4 ºC . Samples were removed halfway through the first 4 ºC phase and briefly stored on ice. A master mix of 2 µL 5x SSIV Buffer, 1 µL DTT and 0.5 µL SSIV Reverse Transcriptase per sample was added to

each tube on ice. Samples were placed back in the Thermocycler and the program was allowed to continue to completion. Final samples were diluted with 90 µL RNA-free water before storage at -20ºC.

The expression of target sequences listed in table 4 were determined with SybrGreen reagents in a QuantStudio 3 (Thermo Fisher Scientific). Briefly, 2 µL of cDNA was mixed with 8µL of prepared master mix (Table 3) and plated in a 96-well plate.

Table 3: Table of reagents for qPCR master mix for samples with a final volume of 10 µL

Reagent	**Volume**
RNase free-water	4.8 µL
5x colorless reaction buffer (Promega)	2.0 µL
dNTP	0.2 mM
Forward primer (IDT)	0.5 µM
Reverse primer (IDT)	0.5 µM
Sybr Green	1.25 µM
ROX (Biotium)	0.5 µM
GoTaq DNA Polymerase (Promega)	0.05 u

Technical replicates were performed for every sample and gene to ensure consistency in pipetting technique. The 96-well plate was covered with a plastic membrane and processed with the following program; 2 minutes at 50ºC followed by 2 minutes at 94ºC, then 40 continuous cycles with three, 30 second stages at 94ºC, 55ºC, and 72ºC. Fold change values were calculated using the $2^{-\Delta\Delta cT}$ method on averaged technical replicates with glyceraldehyde 3-phosphate dehydrogenase (GAPDH) as an internal reference. All statistics were performed in R Studio and were assessed for normality and heteroscedasticity using the functions included in MuMInUtilities library of R Studio prior to a two-way ANOVA to test for differences in fold-change by exposure time and treatment. Westfall and Tukey *post hoc* tests were applied appropriately to assess for differences in treatment groups and controls or exposure time (α=0.05).

Table 4: Target genes for proinflammatory molecules in human keratinocytes (Xu et al., 2018).

Gene	Direction	Sequence
GAPDH*	Forward	5’-TGT TGC CAT CAA TGA CCC CTT-3’
	Reverse	5’-CTC CAC GAC GTA CTC AGC G-3’
CCL2	Forward	5’-CAG CCA GAT GCA ATC AAT GCC-3’
	Reverse	5’-TGG AAT CCT GAA CCC ACT TCT-3’
CCL4	Forward	5’-AAG CTC TGC GTG ACT GTC CT-3’
	Reverse	5’-GAC TTG CTT GCC TCT TTT GG-3’
CXCL2	Forward	5’-GCA GGG AAT TCA CCT CAA GA-3’
	Reverse	5’-GGA TTT GCC ATT TTT CAG CA-3’
Connexin43	Forward	5’-TCA AGC CTA CTC AAC TGC TGG-3’
	Reverse	5’-TGT TAC AAC GAA AGG CAG ACT G-3’
IL-1α	Forward	5’-ATC ATG TAA GCT ATG GCC CAC T-3’
	Reverse	5’-CTT CCC GTT GGT TGC TAC TAC-3’
IL-1β	Forward	5’-CTC GCC AGT GAA ATG ATG GCT-3’
	Reverse	5’-GTC GGA GAT TCG TAG CTG GAT-3’
IL-6	Forward	5’-AAATTCGGTACATCCTCGACGG-3’
	Reverse	5’-GGAAGGTTCAGGTTGTTTTCTGC-3’
IL-8	Forward	5’-TTT TGC CAA GGA GTG CTA AAG A-3’
	Reverse	5’-AAC CCT CTG CAC CCA GTT TTC-3’
MIF	Forward	5’-GTT CCT CTC CGA GCT CAC C-3’
	Reverse	5’-TGC TGT AGG AGC GGT TCT G-3’
MMP1	Forward	5’-AGT GAC TGG GAA ACC AGA TGC TGA-3’
	Reverse	5’-GCT CTT GGC AAA TCT GGC CTG TAA-3’
MMP3	Forward	5’-AGC AAG GAC CTC GTT TTC ATT-3’
	Reverse	5’-GTC AAT CCC TGG AAA GTC TTC A-3’
MMP9	Forward	5’-AGA CGG GTA TCC CTT CGA CG-3’
	Reverse	5’-AAA CCG AGT TGG AAC CAC GAC-3’
COX-2	Forward	5’-GTG CAA CAC TTG AGT GGC TAT-3’
	Reverse	5’-AGC AAT TTG CCT GGT GAA TGA T-3’
S100A8	Forward	5’-ATG CCG TCT ACA GGG ATG AC-3’
	Reverse	5’-ACG CCC ATC TTT ATC ACC AG-3’
S100A9	Forward	5’-GGT CAT AGA ACA CAT CAT GGA GG-3’
	Reverse	5’-GGC CTG GCT TAT GGT GGT G-3’
S100A12	Forward	5’-CCA ATA CTC AGT TCG GAA GGG G-3’
	Reverse	5’-GCA ATG GCT ACC AGG GAT ATG AA-3’
TLR-4	Forward	5’-TTG GGA CAA CCA GCC TAA AG-3’
	Reverse	5’-TGC CAT TGA AAG CAA CTC TG-3’
TNF-α	Forward	5’-ATG AGC ACT GAA AGC ATG ATC C-3’
	Reverse	5’-GAG GGC TGA TTA GAG AGA GGT C-3’

Mus musculus Studies

IACUC and animal husbandry

IACUC protocol was strictly adhered to for this study. Prior approval was obtained under AUP 2019-0271-IBT for the use of SKH1-Elite hairless mice in assessing the effects of topically applied photodegraded polycyclic aromatic hydrocarbons. Animals used in this study were housed at the TAMUK College of Pharmacy vivarium.

Preparation of photodegraded anthracene

A 200 ppm solution of anthracene (Sigma-Aldrich 99%) in acetone (Fisher Chemical) was made with autoclaved glassware and glass Pasteur pipettes. The final solution was added to a 40 mL round-bottom quartz flask with a glass plug for photodegradation. 15mL aliquots were taken for each time point at 0, 1, 4, 8, and 24 hours degradation in the Suntest CPS+ instrument (Atlas). All photodegraded samples were stored in sterile borosilicate vials at 4^{o}C and covered with aluminum foil and a parafilm seal.

Application of treatment to Mus musculus

Pure acetone was used for both the high and low dose control treatments. Anthracene and photodegraded anthracene treatments and control were applied dropwise to the dorsal skin of nude mice (SKH-1) with a glass Pasteur pipette. Trials included 2 mice per treatment. On day 1, 200 µL of the high stimulus treatment (200 ppm) degraded PAH in acetone was applied for treatment groups and acetone was applied for negative controls. Low stimulus treatments (10 ppm) were applied daily on days 7 through 21. Images of any visible abnormalities were noted and photographed during the duration of the treatment. On day 22, all mice were sacrificed according to IACUC protocol with CO_2 inhalation and cervical dislocation. The dorsal skin was removed with a scalpel, and four, 8 mm punch biopsies were taken per mouse. One biopsy from

the shoulder and another from the hip were flash-frozen in liquid nitrogen and stored at -80^{o}C for gene expression analysis. The remaining two samples were placed in a cassette with a sponge and filter paper and stored immediately in 10% formalin at room temperature for histological analysis. Each biopsy was considered as a replicate for a total of 4 replicates per treatment.

Histological Preparation and Analysis

Mouse biopsies were processed according to the same 14-hour tissue protocol as the three-dimensional cultured skin samples (Table 2). After processing, biopsies were cut in half and embedded in paraffin wax using a Histostar (Thermo Scientific), and cross-sections were made with Leica microtome. All samples were stained with a standard hematoxylin (VWR) and eosin (VWR) protocol and analyzed according to the previously mentioned ImageJ analysis for epidermal thickness.

An additional set of 5 µm slides were stained for connexin43 (Miltenyi Biotec) with donkey anti-rabbit primary antibodies according to the previously mentioned standard protocol (Wang et al., 2016). Secondary antibody staining was done using a green anti-donkey Alexa Fluor antibody (488nm). Three fluorescent images were taken per histological sample and both green and DAPI filters and merged in ImageJ. Exposure time was consistent for each image and sample. To quantify the fluorescence intensity, each image was converted to an 8-bit image and the threshold was set to 225/250. The lasso function was used to normalize the fluorescence intensity of green fluorescence to the area for each image, and all images per sample were averaged. Statistics were performed in R Studio with MuMin utilities and multcomp libraries. A one-way ANOVA with Tukey's *post hoc* test was used to assess for significance between degradation treatments and control samples ($\alpha = 0.05$).

Quantification of Gene Expression with RT-qPCR

Punch Biopsy samples were thawed from -80^{o}C and immediately incubated with 3.8% ammonium thiocyanate (Fisher chemical) in DPBS for 30 minutes (Clemmensen et al, 2009). Epidermal cells were carefully scraped off with a sterile razor and quickly transferred to a 2 mL centrifuge tube with 500 µL Trizol Reagent (Ambion by Life Technologies) and 100 µL glass beads (1mm diameter) and stored at -80^{o}C. RNA extraction was performed according to the previously mentioned standard protocol with an additional homogenization step. Samples were violently homogenized for two 1.5 minute rounds in a microtube homogenizer (bertin technologies) before proceeding to the chloroform step. cDNA was synthesized according to the same in-house protocol using MiniAmp Plus Thermal Cycler (Thermo Fisher Scientific).

Table 5: Target genes for proinflammatory molecules in *Mus musculus* keratinocytes (Xu et al., 2018).

Gene	**Direction**	**Sequence**
GAPDH*	Forward	5’- TGA CAT CAA GAA GGT GGT GAA GC-3’
	Reverse	5’- CCC TGT TGC TGT AGC CGT ATT C-3’
Ccl2	Forward	5’- AGG TCC CTG TCA TGC TTC TG-3’
	Reverse	5’- TCT GGA CCC ATT CCT TCT TG -3’
Ccl4	Forward	5’- TGT CTG CCC TCT CTC TCC TC-3’
	Reverse	5’- GTC TGC CTC TTT TGG TCA GG-3’
Cxcl2	Forward	5’- AGT GAA CTG CGC TGT CAA TG-3’
	Reverse	5’- TTC AGG GTC AAG GCA AAC TT -3’
Connexin 43	Forward	5’- ACA GCG GTT GAG TCA GCT TG-3’
	Reverse	5’- GAG AGA TGG GGA AGG ACT TGT-3’
IL-1α	Forward	5’- GCA ACG GGA AGA TTC TGA AG-3’
	Reverse	5’- TGA CAA ACT TCT GCC TGA CG-3’
IL-1β	Forward	5’- TGT GAA ATG CCA CCT TTT GA-3’
	Reverse	5’- TGT CCT CAT CCT GGA AGG TC-3’
IL-6	Forward	5’- CTG ATG CTG GTG ACA ACC AC-3’
	Reverse	5’- CAG AAT TGC CAT TGC ACA AC-3’
Mif	Forward	5’- GCC AGA GGG GTT TCT GTC G-3’
	Reverse	5’- GTT CGT GCC GCT AAA AGT CA-3’
Mmp1	Forward	5’- CTT TGA GGA GGA AGG CGA TAT T-3’
	Reverse	5’- CCA GTT CAT GAG CCG TAA CA-3’
Mmp3	Forward	5’- TCT GAA GGA GAG GCT GAC ATA-3’
	Reverse	5’- TGA GCA GCA ACC AGG AAT AG-3’
Mmp9	Forward	5’- GAC TAC GAT AAG GAC GGC AAA T-3’

	Reverse	5’- GGG CAG AAG CCA TAC AGT TTA-3’
COX-2	Forward	5’- TGA GCA ACT ATT CCA AAC CAG C-3’
	Reverse	5’- GCA CGT AGT CTT CGA TCA CTA TC-3’
S100A8	Forward	5’- AAA TCA CCA TGC CCT CTA CAA G-3’
	Reverse	5’- CCC ACT TTT ATC ACC ATC GCA A-3’
S100A9	Forward	5’- ATA CTC TAG GAA GGA AGG ACA CC-3’
	Reverse	5’- TCC ATG ATG TCA TTT ATG AGG GC-3’
TLR-4	Forward	5’- ATG GCA TGG CTT ACA CCA CC-3’
	Reverse	5’- GAG GCC AAT TTT GTC TCC ACA-3’

The target genes listed in table 5 were analyzed by qPCR in QuantStudio 3 (Thermo Fisher Scientific) using glyceraldehyde 3-phosphate dehydrogenase (GAPDH) as an internal reference. Relative gene expression was calculated by computing fold change values from the $2^{-\Delta\Delta cT}$ method. Statistics were performed in R Studio with MuMin utilities and multcomp libraries and a one-way ANOVA with Tukey’s *post hoc* test was used to assess for significance between degradation treatments and control samples ($\alpha = 0.05$).

3. RESULTS

Chemical Analysis of Photodegraded Anthracene

Chemical Analysis with GC-MS

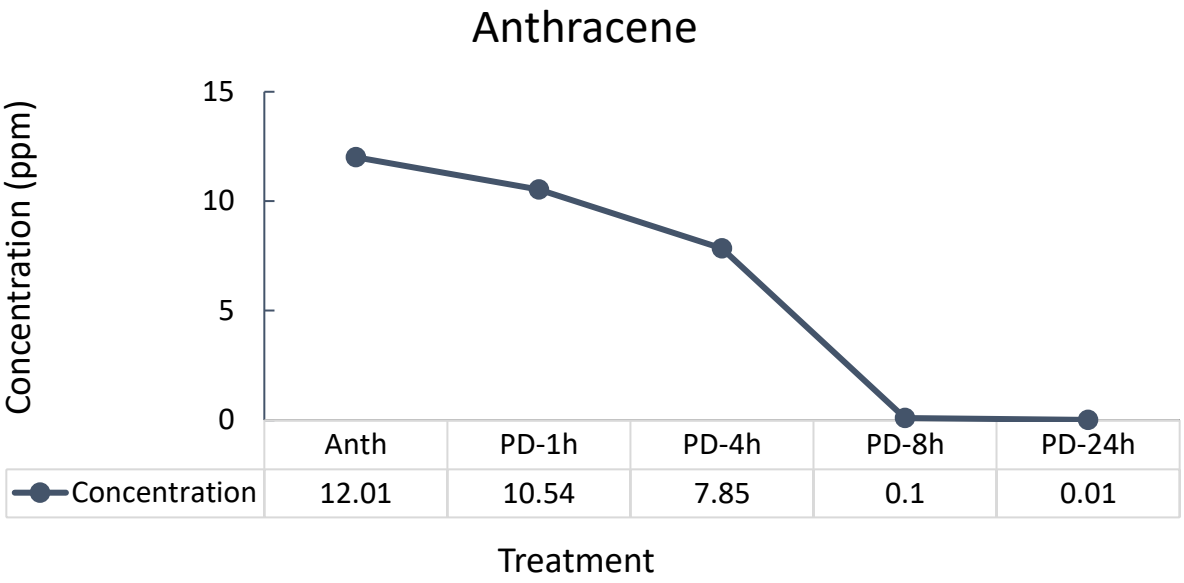

Figure 2: Concentration of anthracene as determined by GC-MS standard curve calculation for anthracene in acetone and photodegraded anthracene treatments at 1-hour, 4-hour, 8-hour, and 24-hours.

The concentration of anthracene in photodegraded treatments was determined by gas chromatogram and mass-spectroscopy analysis (Thermo Scientific TSQ 9000 EVO Triple Quadruple GC-MS/MS) with selected ion monitoring (SIM) mode (Figure 2). Anthracene was demonstrated to degrade within the studied timepoints and decreased most meaningfully between 4-hour and 8-hour timepoints from 7.85 ppm and 0.10 ppm respectively. The starting concentration of nondegraded anthracene in acetone solution was 12.01 ppm and the final concentration at 24-hour photodegradation was 0.01 ppm.

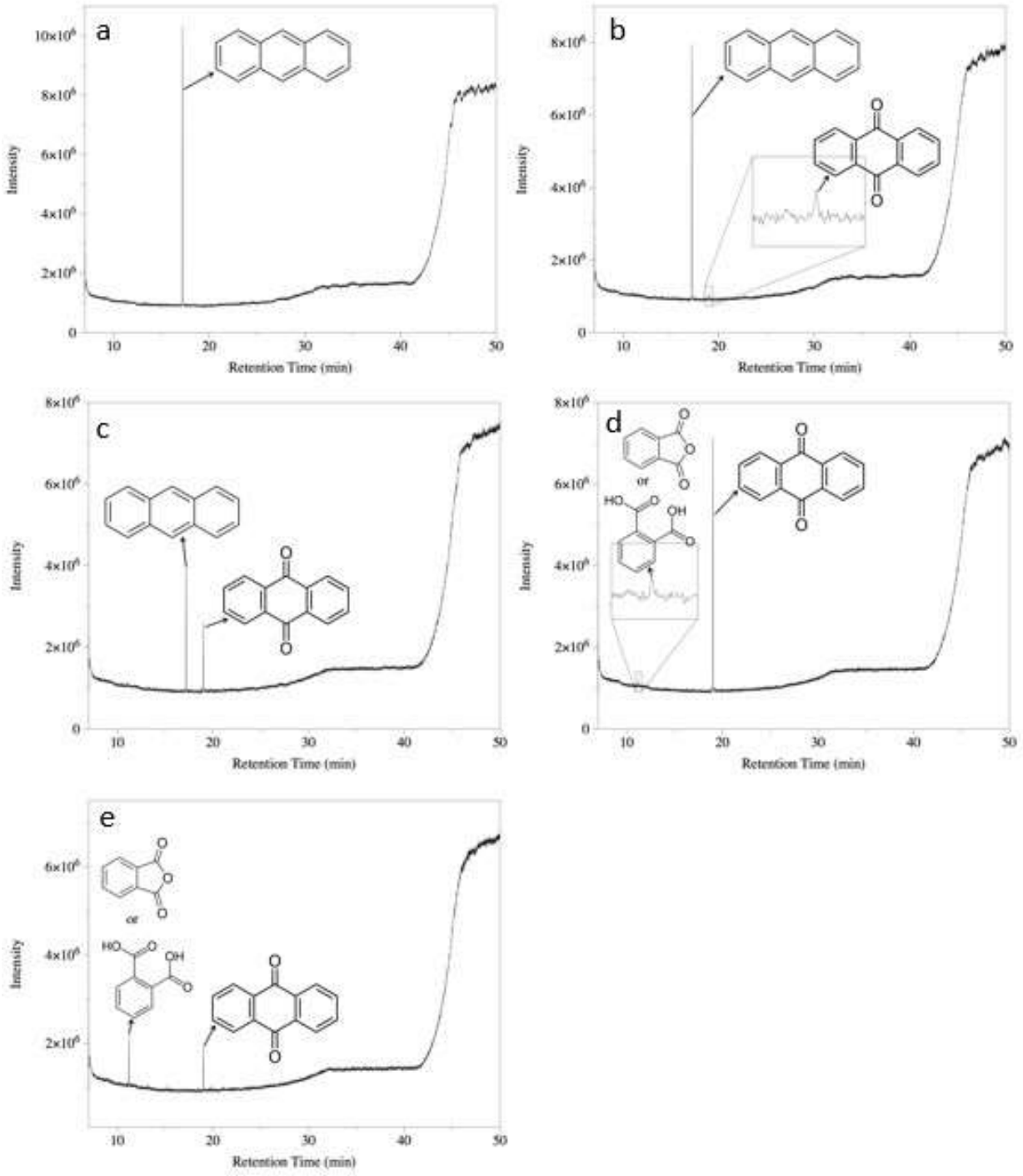

Figure 3: Chromatograms for anthracene (a) and photodegraded anthracene in acetone at 1-hour (b), 4-hour (c), 8-hour (d), and 24-hours (e).

The chemical components of anthracene (a) and 1, 4, 8, and 24-hour photodegraded anthracene (b-e) treatments were analyzed with gas chromatography with chemical comparisons

made using a NIST database (Figure 3). Anthracene was identified in nondegraded, 1, and 4-hour photodegraded samples (a-c). 1,9-anthraquinone is present in 1-hour photodegradation samples and all subsequent solutions (b-e). Phthalic acid or phthalic acid anhydride is present in 8 and 24-hour photodegraded samples (d-e).

Cellular Studies

Migration Assay

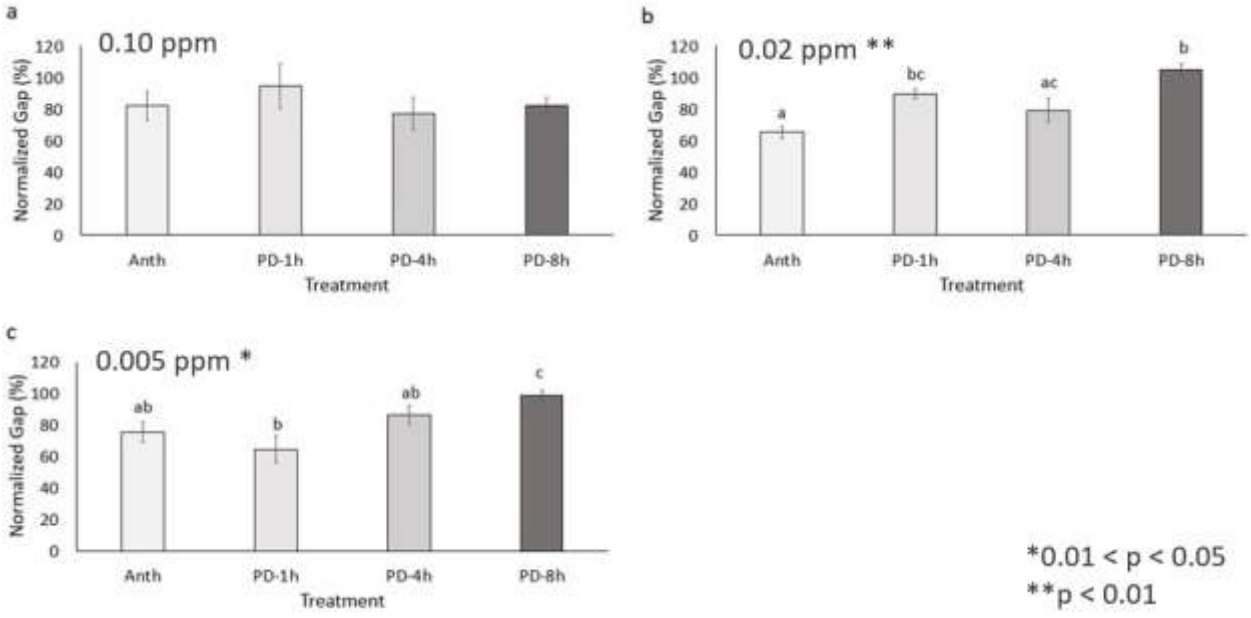

Figure 4: Keratinocyte migration with anthracene and photodegraded anthracene treatments at starting concentrations of 0.1 ppm (a), 0.02 ppm (b), and 0.005 ppm (c). Scratches were made through monolayer keratinocytes and imaged before and after 24 hours of exposure to treatment. Percent gap closure was calculated for treatments and control and plotted as the normalized gap closure. ($p < 0.05$, $n = 6$).

Keratinocytes exposed to anthracene and photodegraded anthracene products showed different migration capabilities as exemplified by a monolayer scratch assay (Figure 4). Normalized gap closure was calculated by dividing the computed gap closure for treatments by the gap closure of control samples for each trial. Similar trends in migration were seen for photodegradation timepoints across two tested concentrations of 0.02 ppm, and 0.005 ppm with

the exception of 0.1 ppm in which no trend was detected among gap closure between photodegraded treatments. The trends in 0.02 ppm and 0.05 ppm show an increase in normalized gap closure as photodegradation time increases, where normalized gap closures were higher in samples exposed to 8-hour photodegraded anthracene than unphotodegraded anthracene for 0.02 ppm and 0.005ppm ($p = 0.00291$, $p = 0.0141$).

The difference in normalized gap closure was significant for anthracene treated samples (65.16 ± 3.70%) compared to 8-hour photodegraded anthracene treatments (104.68 ± 4.05%) for 0.02 ppm ($p < 0.0001$). Gap closures for 4-hour photodegraded treatments were significantly less than 8-hour photodegraded treatments at only 79.04 ± 7.36% normalized gap closure ($p = 0.00692$).

Normalized gap closures for anthracene treated samples were 75.26 ± 6.47% compared to 98.74 ± 2.63% for 8 hour photodegraded treatments at 0.005 ppm ($p = 0.0637$). Gap closures for 1 hour photodegraded anthracene treatments (64.53 ± 8.64%) were significantly different than 8 hour photodegraded treatments at the same concentration ($p = 0.0109$).

Cytotoxicity Assay

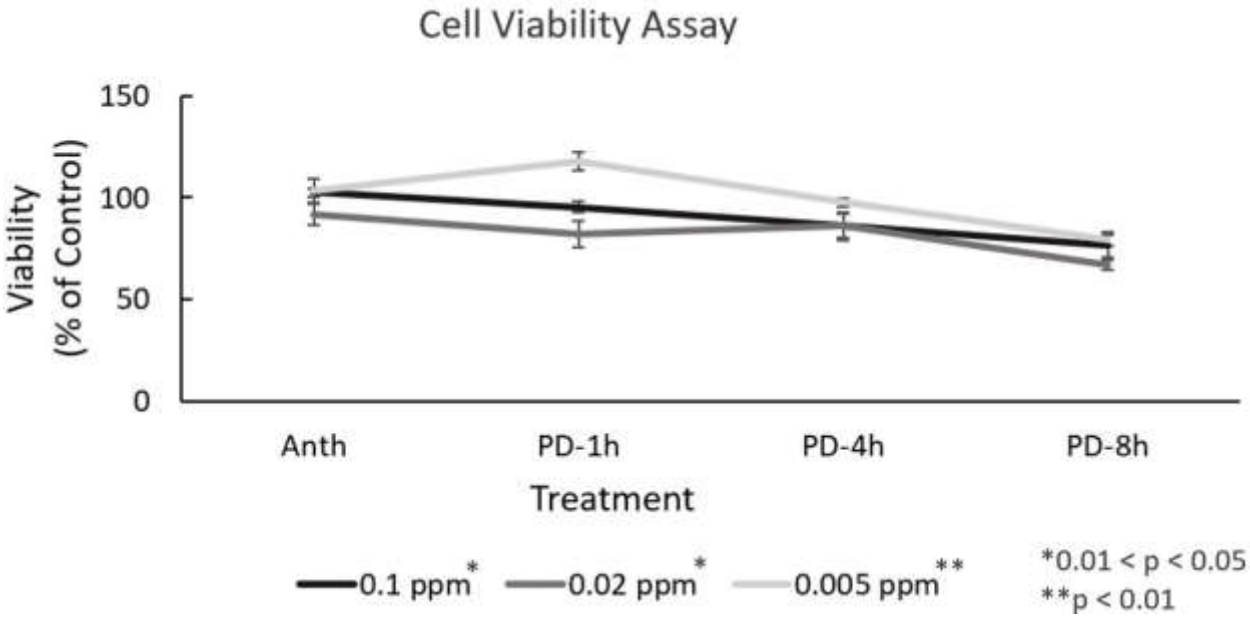

Figure 5: Cytotoxicity assay for HaCaT keratinocytes exposed to anthracene and photodegraded anthracene treatments for 18 hours with dilutions of 0.1 ppm, 0.02 ppm, and 0.005 ppm. Percent viability was calculated by dividing the absorbance at 590nm of treated cells by the absorbance of non-treated cells. ($p < 0.05$, $n = 6$)

An MTT Assay was used to assess the viability of HaCaT keratinocytes treated with anthracene and photodegraded anthracene products (Figure 5). Viability was calculated by dividing the OD at 570nm of treated cells by controls. Anthracene and photodegraded anthracene products had cytotoxic effects on HaCaT Keratinocytes, and longer photodegradation treatments resulted in significantly decreased viability at 0.1 ppm, 0.02 ppm, and 0.005 ppm dilutions ($p = 0.0110$, $p = 0.0442$, $p = 0.000105$).

HaCaT keratinocytes treated with 8-hour photodegraded anthracene had significantly decreased viability (76.98 ± 6.20%) than cells treated with anthracene (102.67 ± 2.01%) and 1-hour photodegraded anthracene (95.25 ± 2.70%) at 0.10ppm ($p = 0.00905$, $p = 0.0472$). At 0.02 ppm concentrations, cells treated with 8-hour photodegraded anthracene had a significantly decreased viability (67.02 ± 2.6%) than cells treated with anthracene (92.02 ± 5.30%) ($p = 0.0355$).

8-hour photodegradation treatments decreased HaCaT viability by as much as 38.95% compared to 1-hour photodegradation treatments ($p < 0.001$), and viability decreased steadily as photodegradation time increased from 1-hour to 8-hour (118.04 ± 4.42%, 97.77 ± 2.02%, 79.09 ± 3.05%) at 0.005 ppm ($p = 0.00414$, $p < 0.001$, $p = 0.0201$).

Three-Dimensional Stratification Assay

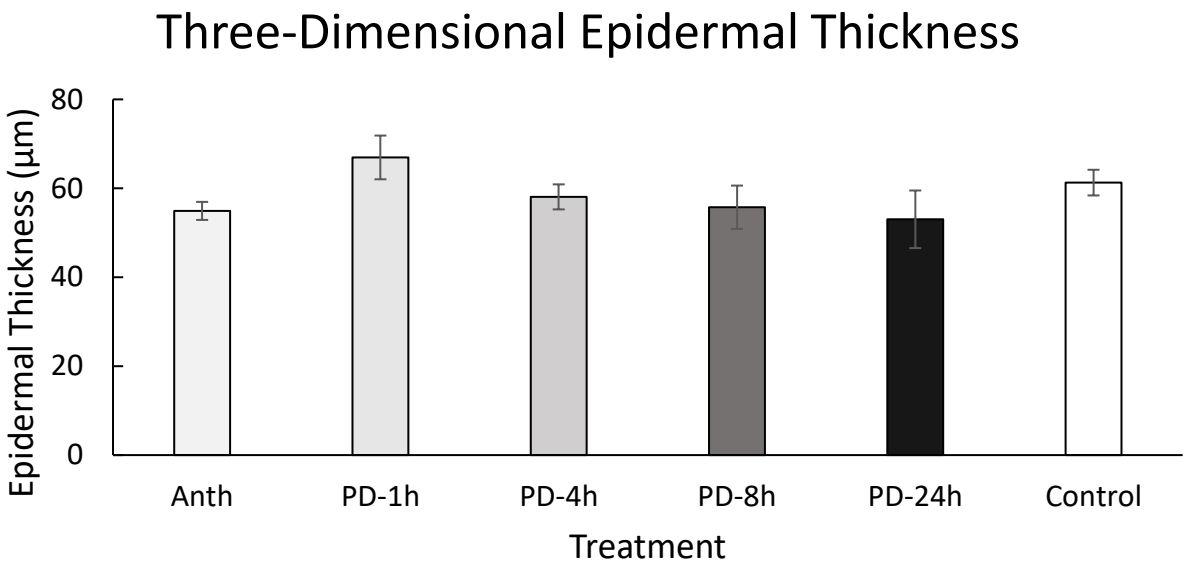

Figure 6: Average epidermal thickness of three-dimensional HaCaT keratinocyte cultures stratified with anthracene and photodegraded anthracene treatments (stratified over 14 days with a daily 8 hour exposure). Measurements were calculated by dividing the total epidermal area by the length of sample in ImageJ. Values are expressed as mean ± standard error of the mean. ($p<0.05$, $n = 4$)

HaCat keratinocytes were stratified in anthracene and photodegraded anthracene treatments over 14 days to assess three-dimensional developmental effects (Figure 6). There were no statistically significant differences in epidermal thickness between treatments or control ($p = 0.2683$), however, 1-hour photodegraded treatments (66.94 ± 4.92 µm) were thicker than control samples (61.25 ± 2.89 µm) on average, and all other photodegraded treatments resulted in decreased epidermal thickness compared to control. 24-hour photodegraded treatments resulted in the lowest thickness (53.03 ± 6.47 µm) followed by anthracene (54.92.03 ± 2.03 µm), 8-hour (55.74 ± 4.87 µm) and 4-hour photodegraded treatments (58.07 ± 2.81 µm).

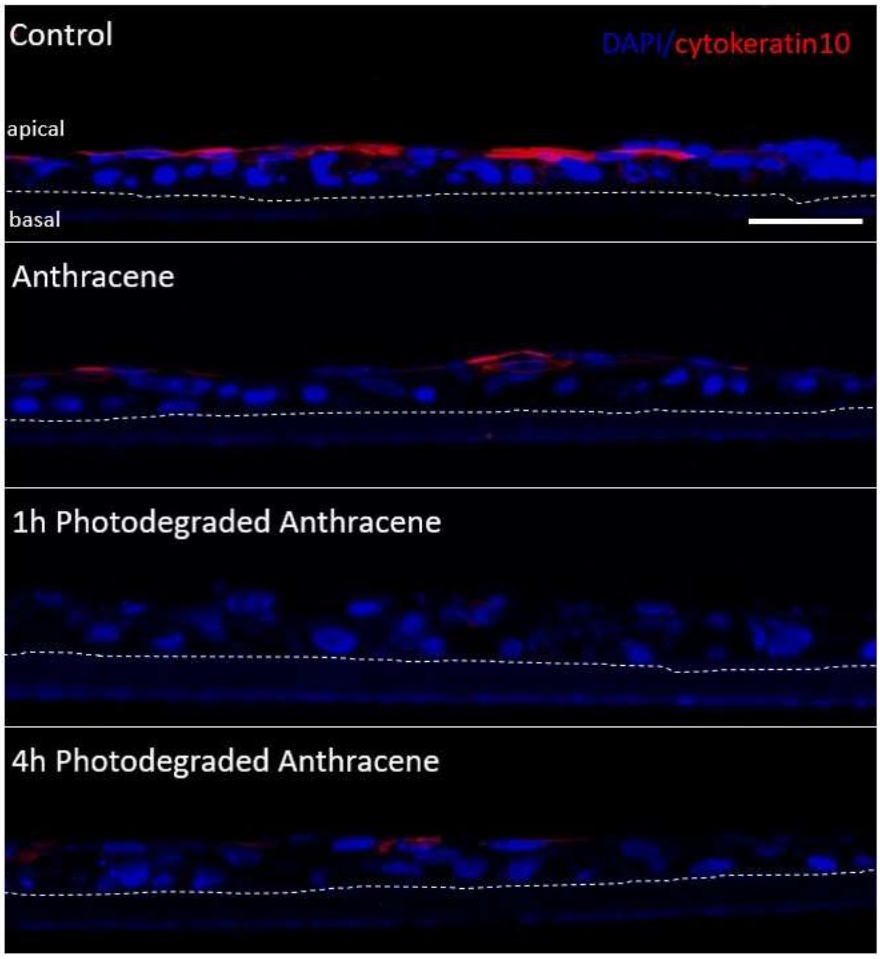

Figure 7: Immunofluorescent staining of cytokeratin 10 in red and DAPI in blue for control (a), anthracene (b), 1-hour (c), and 4-hour (d) photodegraded anthracene treated cells grown for three-dimensional stratification assay.

Cytokeratin10 expression was visualized in three-dimensionally cultured keratinocytes treated with anthracene and photodegraded anthracene treatments (Figure 7). Anthracene and photodegraded anthracene treatments showed a diminished presence of cytokeratin10 in the apical layer as compared to the control.

Quantification of Gene Expression

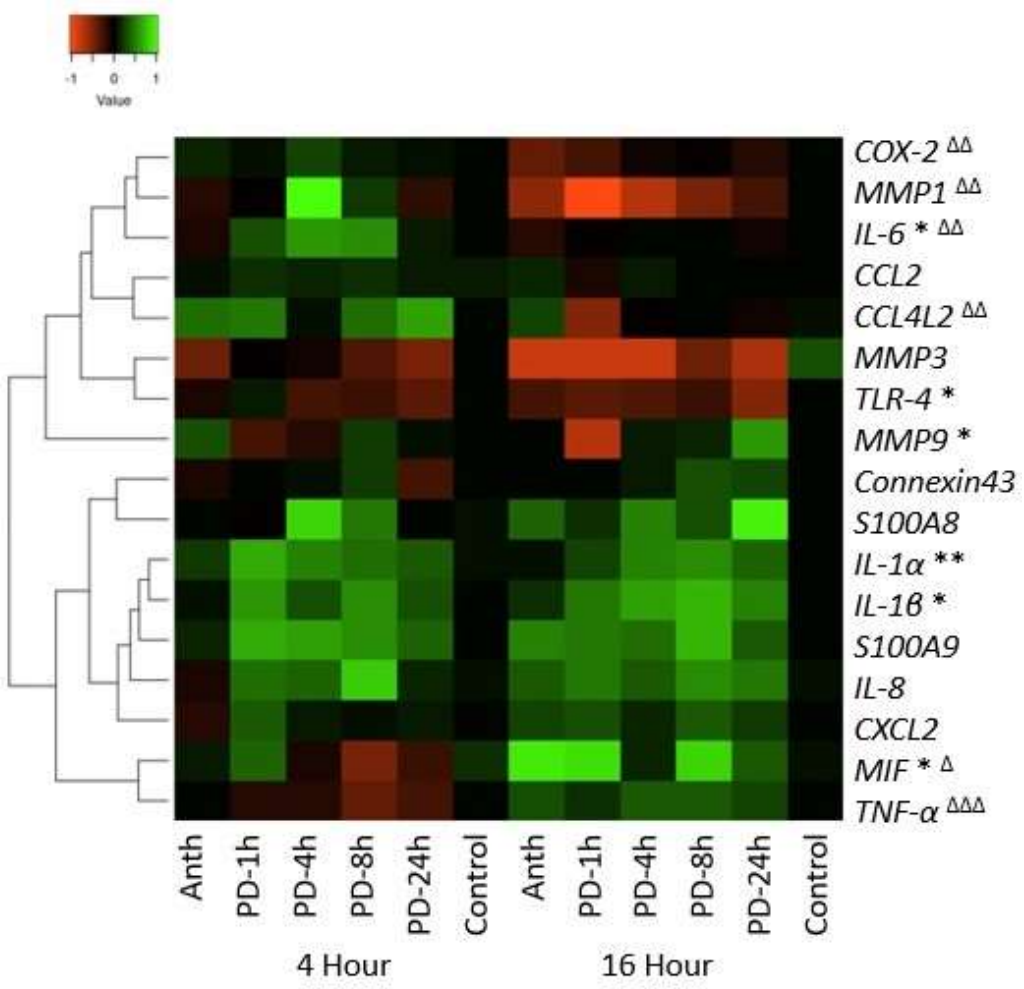

Figure 8: Heatmap of 17 proinflammatory genes for HaCaT keratinocytes exposed to anthracene and photodegraded anthracene treatments for 4 and 16 hours at 0.1 ppm. Values are displayed as the Log(2) of mean expression and are represented as upregulation (green) and downregulation (red) compared to control. (*$0.01 < p < 0.05$, ** $0.001 < p < 0.01$, *** $p < 0.001$ for differences in treatment groups; $^{\Delta}0.01 < p < 0.05$, $^{\Delta\Delta}0.001 < p < 0.01$, $^{\Delta\Delta\Delta}p < 0.001$ for differences in exposure times; n = 6)

HaCaT keratinocytes treated with anthracene and photodegraded anthracene for 4 and 16 hours displayed differential gene expression of 17 proinflammatory cytokines with notable differences between both treatment groups and exposure times (Figure 8). A two-way ANOVA showed that *TNF-α, CCL4L2* and *COX-2* fold-change values were significantly different

between exposure times but not treatments ($p < 0.0001$, $p = 0.0003$, $p < 0.0001$). *TLR-4*, *IL-1α*, *IL-1β*, and *MMP9* expression levels were significantly different for treatments but not exposure times ($p = 0.0212$, $p = 0.00670$, $p = 0.0110$, $p = 0.0150$). *MMP1* was expressed at control levels in 4 hour exposures ($p = 0.0543$), and downregulated at 16 hours ($p = 0.0183$). *IL-6* and *MIF* fold-change values were significantly different for exposure time ($p = 0.00390$, $p = 0.0001$) and treatment ($p = 0.0459$, $p = 0.0228$). *IL-1α* and *IL-1β* displayed similar expression trends in fold-change values between treatments for both 4 hour ($p = 0.0784$, $p = 0.232$) and 16 hour exposure times ($p = 0.0887$, $p = 0.083$).

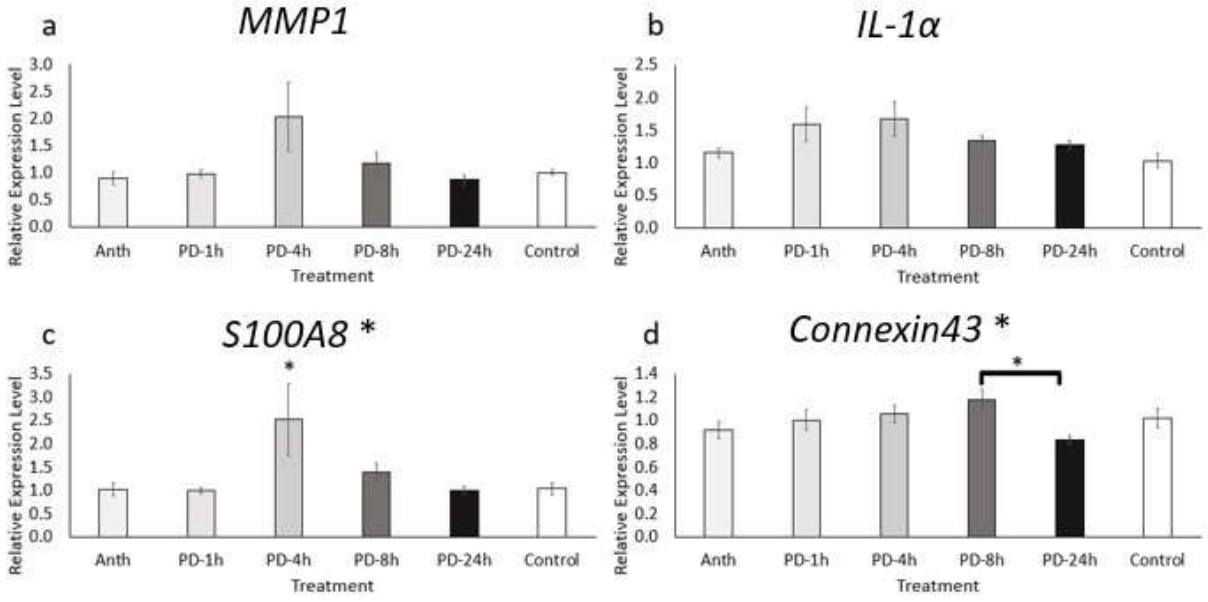

Figure 9: Relative expression level of *MMP1* (a), *IL-1α* (b), *S100A8* (c), and *Connexin43* (d) for HaCaT keratinocytes exposed to anthracene and photodegraded anthracene treatments for 4 hours at 0.1 ppm. Values are presented as the mean ± standard error of the mean. (*$0.01 < p < 0.05$, ** $0.001 < p < 0.01$, *** $p < 0.001$, $n = 6$)

A one-way ANOVA was used to compute differences in fold-changes by treatment for each gene with a 4 hour exposure. Four genes were differentially expressed under 4 hour exposures to photodegraded anthracene treatments (Figure 9). 4-hour photodegradation

treatments increased gene expression for *MMP1*, *IL-1α*, and *S100A8* compared to controls (p = 0.0540, p = 0.0784, p= 0.0210). *Connexin43* gene expression was reduced for 24-hour photodegraded treatments compared to 8-hour photodegraded treatments, but not control (p = 0.0432).

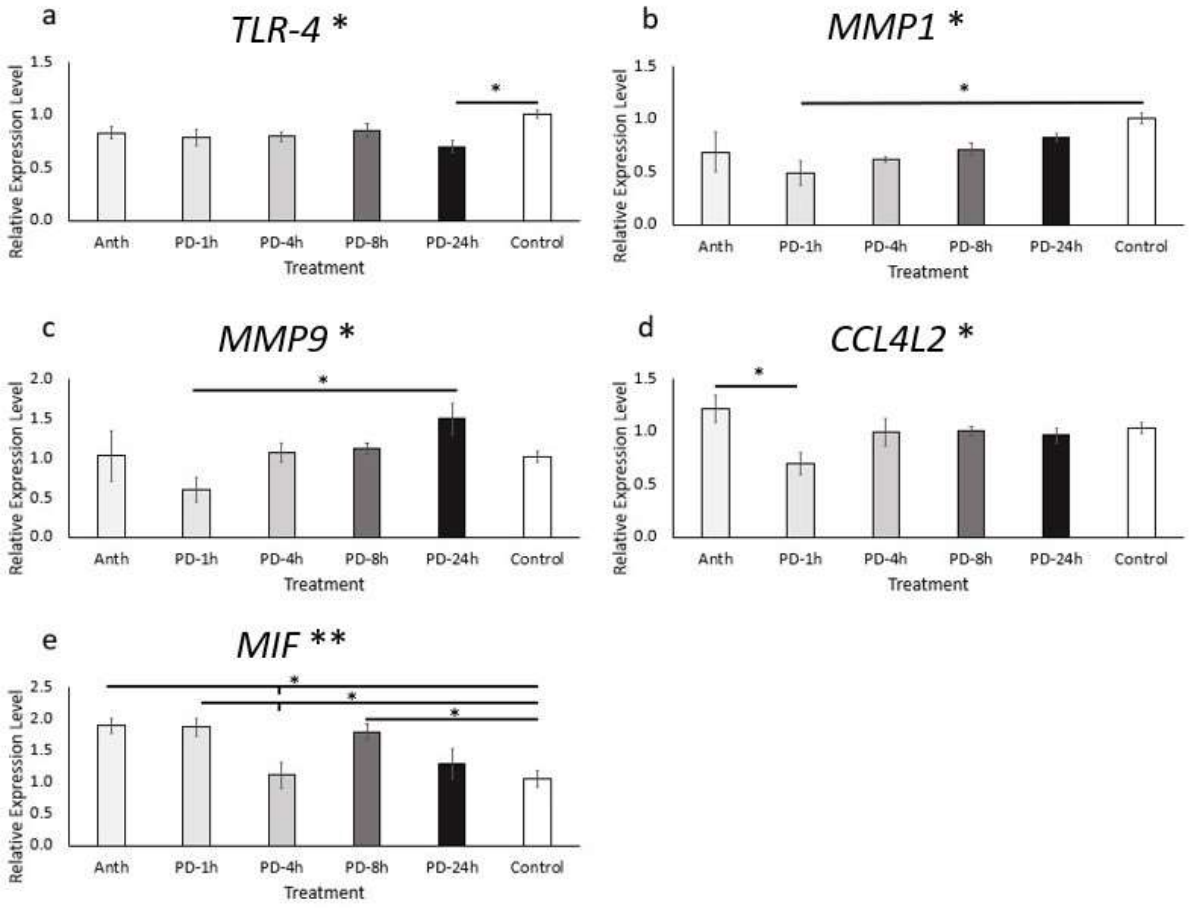

Figure 10: Relative expression level of *TLR-4* (a), *mmp1* (b), *mmp9* (c), *ccl4l2* (d), and *MIF* (e) for HaCaT keratinocytes exposed to anthracene and photodegraded anthracene treatments for 16 hours at 0.1 ppm dilutions. Values are presented as the mean ± standard error of the mean. (*0.01 < p < 0.05, ** 0.001 < p < 0.01, *** p < 0.001, n = 6)

A one-way ANOVA was used to compute differences in fold-changes by treatment for each gene with a 16 hour exposure. Five genes were significantly differentiated under 16 hour exposures (Figure 10). *TLR-4* (p = 0.0193) expression was significantly different for 24-hour

photodegraded treatments compared to controls ($p = 0.00727$) and all treatments were downregulated on average. *MMP1* expression was similarly downregulated for all treatments ($p = 0.0183$), and 1-hour photodegraded treatments were significantly downregulated than control ($p = 0.01$). Expression levels for *MMP9* ($p = 0.0463$) were significantly different between 24-hour and 1-hour photodegraded treatments where 24-hour photodegraded treatments were upregulated and 1-hour photodegraded treatments were downregulated ($p = 0.0142$). Anthracene induced expression of *CCL4L2* compared to 1-hour photodegraded anthracene ($p = 0.00803$) and no treatment groups were significantly different than control. *MIF* was differentially expressed ($p = 0.00121$) in all treatment groups with the exception of 4-hour and 24-hour photodegraded anthracene. 4-hour and control fold-changes were significantly less than anthracene treatments ($p = 0.0306$, $p = 0.0164$) and 1-hour photodegraded anthracene treatments ($p = 0.0369$, $p = 0.0200$). 8-hour photodegraded anthracene also elicited overexpression of *MIF* compared to control values ($p = 0.0474$).

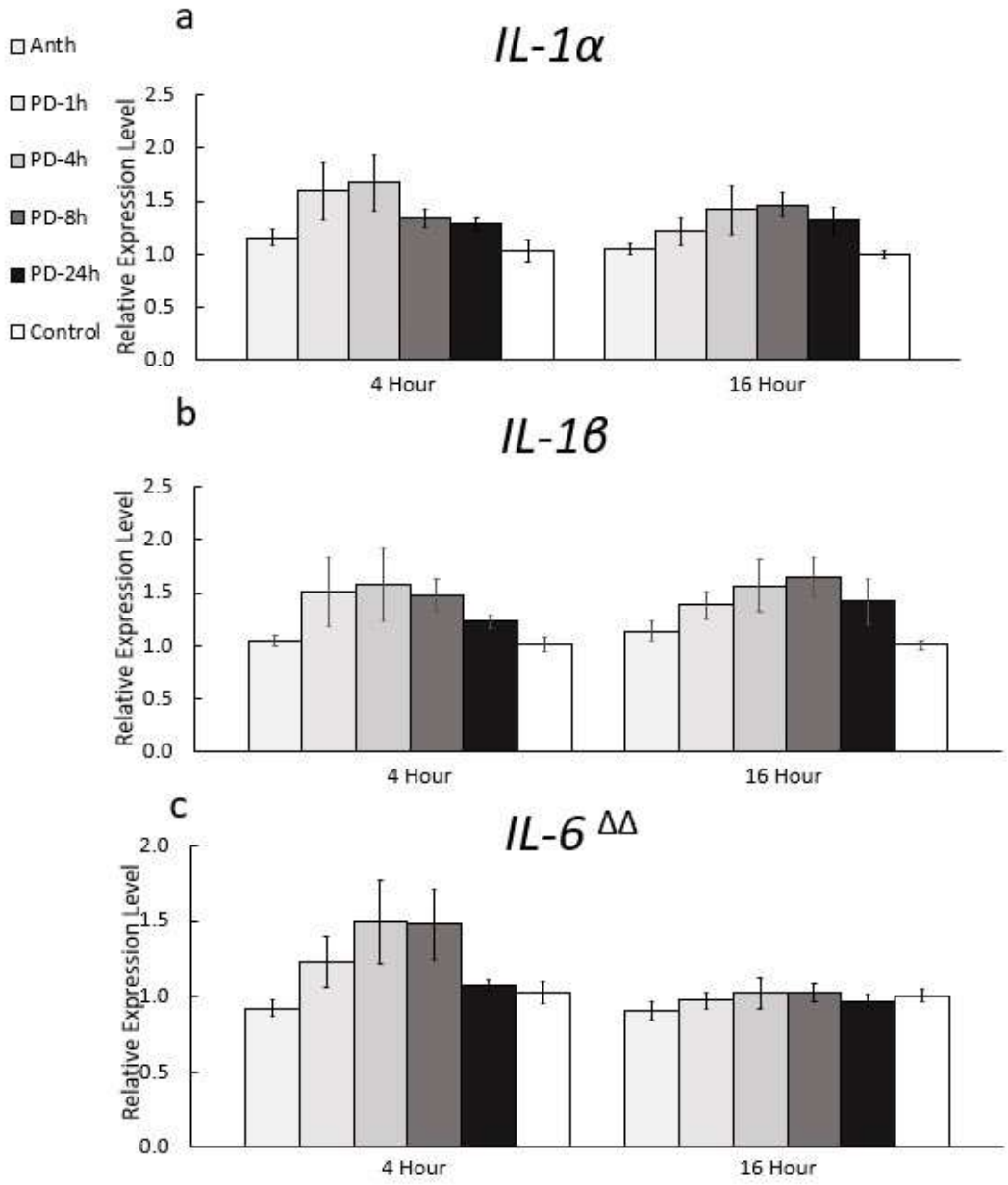

Figure 11: Relative expression level of *IL-1α* (a), *IL-1β* (b), and *IL-6* (c) for HaCaT keratinocytes exposed to anthracene and photodegraded anthracene treatments for 4 and 16 hours at 0.1 ppm. Values are presented as the mean ± standard error of the mean. ($p<0.05$, $n = 6$)

Three genes demonstrated temporal and treatment-related trends for HaCaT keratinocytes treated for 4 and 16 hours (Figure 11). Although not significant under one-way ANOVA computations, *IL-1α* (a) and *IL-1β* (b) expression increased steadily above control values between anthracene and 4-hour photodegraded treatments for both exposure times. *IL-6* (c) also

demonstrated an increasing linear trend in expression for 4 hour exposures, but this trend was diminished for 16 hour exposures. A two-way ANOVA showed a statistically significant difference in fold-changes by exposure time ($p = 0.00390$) and treatments ($p = 0.0459$) for *IL-6* expression.

Mus musculus Studies

Histological Analysis

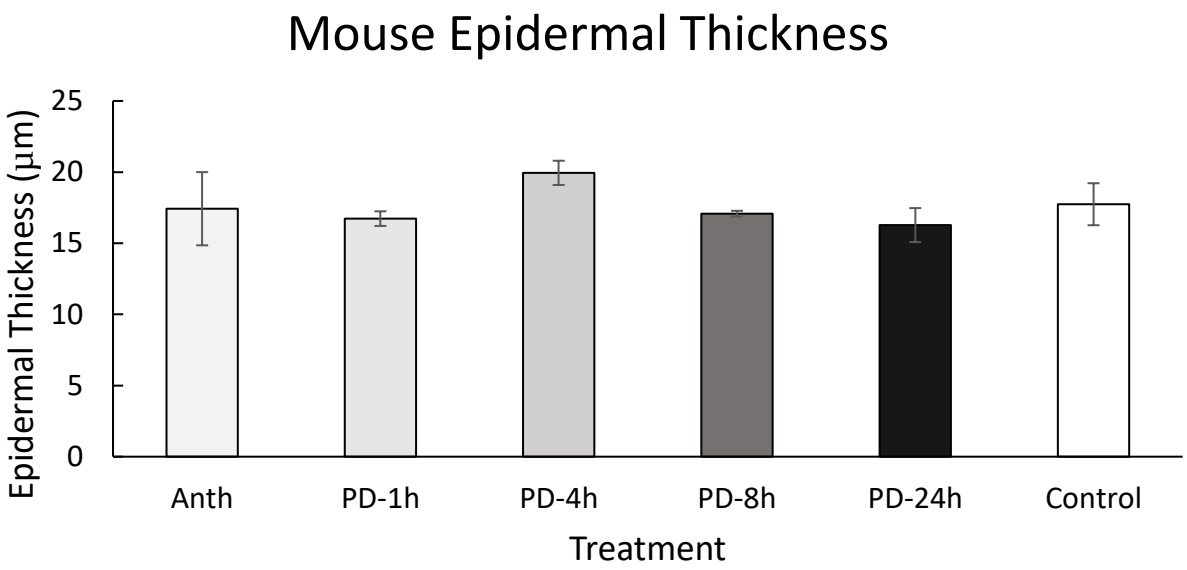

Figure 12: Mouse epidermal thickness for SKH1-Elite mice treated daily with 10 ppm anthracene and photodegraded anthracene in acetone. Measurements were calculated by dividing the total epidermal area by the length of the sample in ImageJ. Values are expressed as mean ± standard error of the mean. ($p<0.05$, $n=4$)

Epidermal thickness for SKH1-Elite mice was determined by the measurement of histological samples (Figure 12). There were no statistically significant differences between treatment and control values for epidermal thickness ($p= 0.510$), however, 4-hour photodegraded anthracene treatments showed modest increases in thickness (19.95 ± 0.85 µm) compared to control samples (17.74 ± 1.48 µm). 1-hour, 8-hour, and 24-hour photodegraded treatments demonstrated a reduced thickness (16.73 ± 0.51 µm, 17.08 ± 0.20 µm, 16.28 ± 2.38 µm) and

anthracene alone treatments exhibited an epidermal thickness similar to control treatments (17.43 ± 2.57 µm).

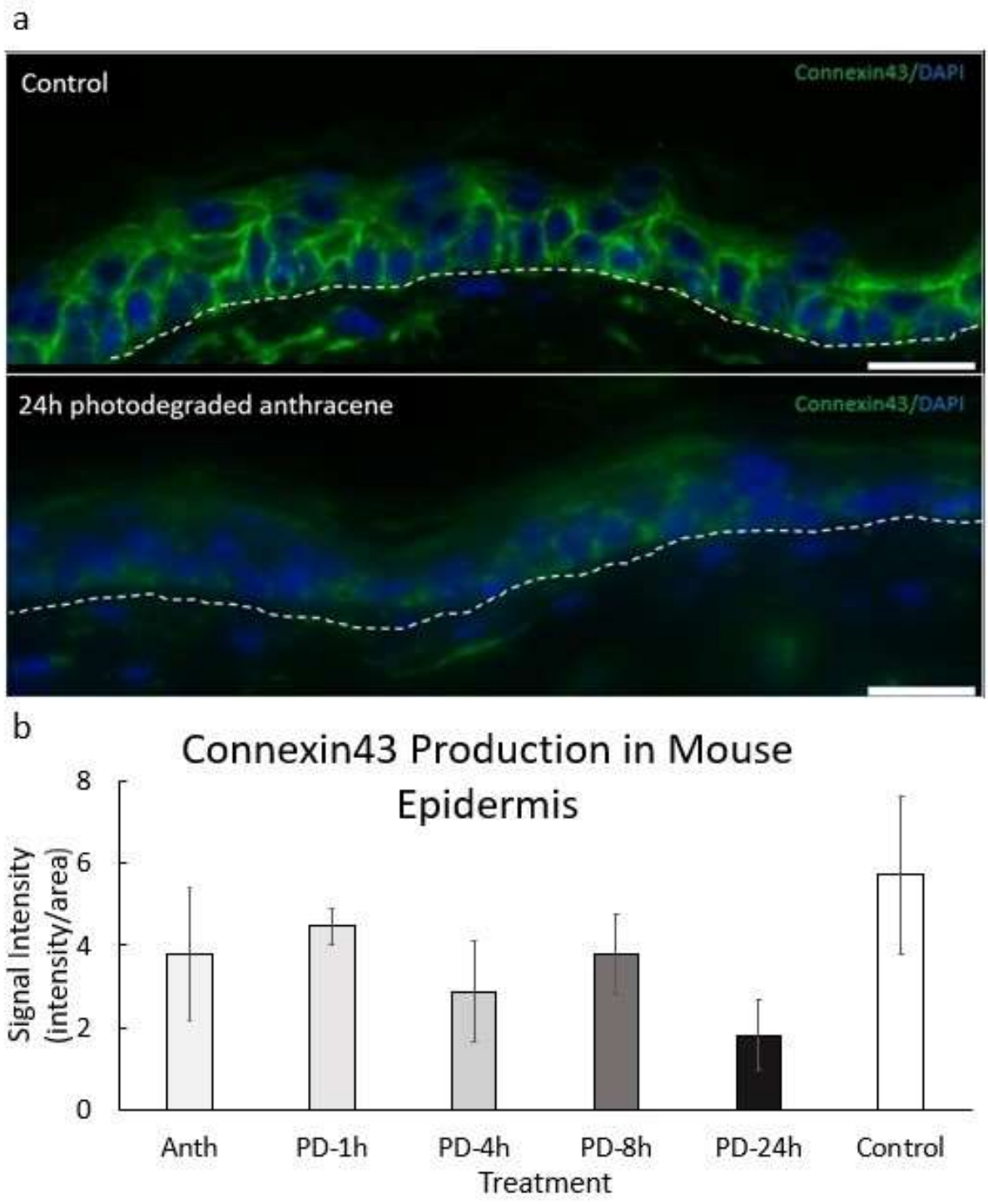

Figure 13: The expression of Connexin43 in SKH1-Elite mouse epidermis was evaluated by immunofluorsecent staining of Connexin43 (green) and DAPI (blue) for control and 24-hour

photodegraded anthracene (a). Signal intensity was measured and normalized to epidermal area in ImageJ (b). ($p<0.05$, n = 2)

Connexin43 expression was visualized by immunofluorescence and quantified in SKH1-Elite mouse epidermis after 14 consecutive daily treatments with acetone (control) and photodegraded anthracene in acetone (Figure 13). The greatest difference in signal intensity was observed between control (5.70 ± 0.61) and 24-hour photodegraded treatments (1.82 ± 0.68) followed by 4-hour photodegraded treatments (2.88 ± 0.31). Anthracene and 8-hour photodegraded anthracene treatments had the same fluorescent signal intensity (3.79 ± 1.35, 3.79 ± 0.86).

Quantification of Gene Expression

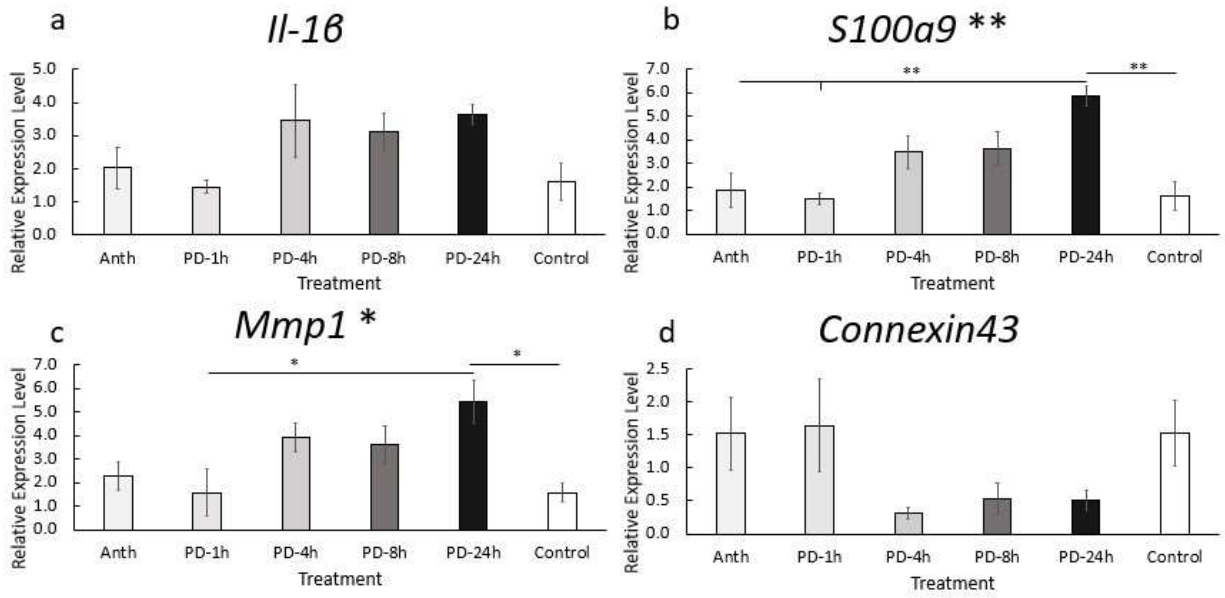

Figure 14: Relative expression level of *Il-1β* (a), *S100a9* (b), *Mmp1* (c), and *Connexin43* (d) for SKH1-Elite mice exposed to anthracene and photodegraded anthracene treatments for 14 consecutive days at 10 ppm. Values are presented as the mean ± standard error of the mean. ($p<0.05$, n = 6)

Mice exposed to daily treatments of anthracene and photodegraded anthracene demonstrated differential gene expression for *Il-1β, S100a9, Mmp1,* and *Connexin43* (Figure 14).

Notable trends in expression between photodegraded treatments include an upregulation in gene expression for *Il-1β* ($p = 0.168$), *S100a9* ($p = 0.00167$), and *Mmp1* ($p = 0.0269$) for 4, 8, and 24-hour photodegraded treatments with corresponding downregulation in *Connexin43* ($p = 0.235$) for the same treatments (Figure 14). *S100a9* expression was upregulated in 24-hour photodegraded anthracene compared to anthracene, 1-hour photodegraded anthracene, and control values ($p = 0.00667$, $p = 0.00301$, $p = 0.00400$). *Mmp1* expression was upregulated in 24-hour photodegraded anthracene compared to 1-hour photodegraded anthracene and control values ($p = 0.0432$, $p = 0.0427$).

4. DISCUSSION

Chemical Analysis of Photodegraded Anthracene

Photodegradation of anthracene produces oxidixed compounds

The results of our chemical analysis confirm that anthracene is non-linearly degraded under UV light over a 24-hour period (Figure 2). The concentration of anthracene was determined for the stock solution as well as the 1 and 4-hour photodegraded samples (Figure 3). However, these anthracene was not detected in the 8 and 24-hour photodegraded samples. Oxidized product formation is first noted at 1-hour photodegradation, and the continuous appearance of this products is confirmed by the appearance of additional peaks in the 4, 8, and 24-hour photodegraded solutions.

The most commonly cited intermediate product in literature is the 1,8 dihydroxyanthraquinone and 9,10-anthraquinone, and our analysis confirms the presence of the latter compound in 1, 4 and 8-hour photodegraded samples (Dąbrowska et al., 2008). These products have a greater absorption at 220 nm and 270-300 nm with a corresponding decrease in absorbance at 250 and 300-400 nm (Dąbrowska et al., 2008). 1,9-anthraquinone causes dermal irritation in rabbits, although the acute dermal toxicity is classified as low (US Environmental Protection Agency, 1998). The 8 and 24-hour photodegraded samples also include peaks that indicate phthalic acid or phthalic anhydride which are likely oxidation products of the anthraquinone (Hassan et al., 2015). Phthalic anhydride quickly hydrolyses to phthalic acid in the presence of water, and the acid form is known to cause skin, eye, and respiratory tract irritation (US Environmental Protection Agency, 2000; Bang et al., 2011).

Phthalic acid and 9,10-anthraquinone are also major products of naphthalene photocatalytic degradation, and naphthalene degradation may produce more of these compounds than

anthracene (Malakahmad et al., 2016). The phototoxicity of naphthalene and other PAHs should be further investigated to understand which PAH intermediates may be of higher concern with dermal exposure.

Cellular Studies

The results of this study support the conclusion that the photodegraded products of anthracene induce a variety of toxic effects in keratinocytes. Cell migration, viability, and proinflammatory gene expression were affected by photodegraded anthracene. In general, exposure to anthracene that was photodegraded for a longer time produced greater cytotoxic responses and was more activating to HaCaT keratinocytes. Gene expression of proinflammatory markers was differentially expressed in all treatment groups, and expression levels were more pronounced in longer photodegradation treatments than unphotodegraded anthracene.

Photodegraded anthracene activates keratinocytes to migrate

Cell migration studies suggest that keratinocytes are more activated by exposure to longer photodegradation treatments when compared to non-photodegraded anthracene (Figure 4). Keratinocytes within an un-wounded epidermis will exhibit a 'balanced' mode with an equal number of proliferating, differentiating, and senescing cells (Roshan et al., 2016). In wound assays, keratinocytes cells along with the gap border switch from a 'balanced' mode to an 'expanding' mode until confluence is achieved (Roshan et al., 2016). This 'expanding' mode requires a coordinated response among the expanding cells at the gap border to achieve efficient migration, and this response is mitigated by proinflammatory markers. Keratinocytes express ample matrix metalloproteinases (MMPs) such as MMP1, MMP2, and MMP9 at wound edges, in addition to cytokines like IL-1, IL-6 and TNF-α (Rodrigues et al., 2019; Woodley et al., 2015; Xiao et al., 2020). Our finding that longer photodegraded treatments exhibit a greater expanding

behavior than un-photodegraded anthracene treatments suggests that the intermediate products in photodegraded anthracene can activate migration. These findings are supported by gene expression analysis which also showed positive trends in *IL-1α* and *IL-1β* production for longer photodegradation treatments at two exposure times (Figure 10). Interestingly, *IL-6* expression followed similarly increasing trends for longer photodegradation treatments in 4-hour exposure times, but this effect was diminished after 16-hours and neither result was significant. *IL-1β*, and *TNF-α* are necessary for the production of *IL-6* and *IL-8* (Gruys et al., 2005). Our results support this, and indicate that *IL-1α* and *IL-1β* are independently expressed from *IL-6* and are influential on keratinocyte migration.

The expression of proinflammatory cytokines and proteinases by keratinocytes is part of the normal wound-healing response to inflammation, and the timely release of cytokines directs a sequential progression beginning with inflammation and hemostasis, to proliferation and remodeling. However, excessive signaling for keratinocyte migration in wound-healing tissue may lead to profuse remodeling and chronic inflammation without appropriate proliferation (Landen et al., 2016; Xiao et al., 2020). Increased cell migration and uncoordinated proliferation can leave adjacent skin barriers more permeable to environmental exposure (Landen et al., 2016). Additionally, excess scar formation may result from the faster migration of keratinocytes in wound-healing is not necessarily favorable for every type of epidermal damage. Our results suggest that migration does not occur in excess to control values, and we interpret this to mean that the activation of keratinocytes is appropriate in intensity. However, future migration studies that include additional measurements during migration may be necessary to clarify the rate of gap closure over a 24 hour period.

Photodegraded anthracene exhibits greater inhibition of cell viability than anthracene

Cell viability was assessed with an MTT assay after 18 hours of exposure (Figure 5). The average length of the keratinocyte cell cycle is 15.7 hours and is reported to be closer to 24 hours for near-confluent cell culture, therefore 18 hours was used as a representative exposure time to investigate cytotoxic effects (Dover & Potten, 1988; Roshan et al., 2016). Our MTT results support the conclusion that photodegradation increases the cytotoxic effects of anthracene. At all three tested concentrations, 8-hour photodegraded anthracene treatments decreased the viability compared to un-photodegraded products (Figure 5). Keratinocytes make up the outermost layer of the epidermis, and direct cytotoxic effects on these cells can result in an imbalance in the ratio of proliferative and apoptotic cells that supports homeostatic skin barrier. The most common causes of keratinocyte apoptosis include environmental factors such as UV radiation, and genetic susceptibility to diseases like psoriasis or cancer (Raj et al., 2006). Severe epidermal impairments can leave patients susceptible to infection and unable to regulate electrolytes and body temperature. Additionally, an impaired skin barrier may facilitate an irritant contact dermatitis response, and lead to atopic dermatitis with repetitive exposure (Bains, 2018; Ronfard & Barrandon, 2001).

Cytotoxicity can imply that cells are undergoing an apoptotic process, and this process is mediated by cytokines. TNF-α is a notable cytokine that can paradoxically induce keratinocyte proliferation or apoptosis (Kokolakis et al., 2021). Additionally, keratinocyte-derived TNF-α is a signature of chronic phase psoriasis in which keratinocytes proliferate abundantly (Albanesi et al., 2018). In our study, *TNF-α* expression was initially downregulated for 4-hour exposures and upregulated after 16-hours, which may suggest that keratinocytes may be overexpressing *TNF-α* to compensate for the initial cytotoxic effects (Figure 8). These MTT results and gene expression analysis, therefore, suggest that photodegraded anthracene may impair the developed epidermal

barrier via direct cytotoxic effects on keratinocytes (Figure 5). Taken with our migration results, these cellular studies imply that longer photodegradation times have both a cytotoxic and activating effect. In a developed skin barrier, these features have the potential to disrupt the epithelial barrier.

Photodegraded anthracene initiates a similar but more severe proinflammatory gene response than anthracene in keratinocytes

Keratinocytes are the first cell type in the epidermis to interact with environmental stressors, and they respond to stressors by initiating inflammatory repones through molecules like cytokines, chemokines, upstream receptors, and downstream effector molecules. 17 proinflammatory molecules were previously identified for their importance in initiating an inflammatory response in keratinocytes (Xu et al., 2014). Not all markers are implicated in overlapping pathways, and the purpose of screening these consortia of molecules is to identify a putative pathway that is implicated in the keratinocyte inflammatory response to photodegraded anthracene. Our study assessed both early (4-hour) and sustained (16-hour) inflammation to understand the temporal response of keratinocytes.

Keratinocytes direct the initial inflammatory pathway through a number of different cascades that are triggered by several different receptors (Landen et al., 2016). These pattern recognition receptors (PRR) include toll-like receptors (TLR) and NOD-like receptors (NLR) and alarmins (Klicznik et al., 2018). Alarmin molecules including defensins, S100 proteins, and heat-shock proteins are also released by damaged cells, chemical exposure, and UV radiation. (Klicznik et. al., 2018). Both TLR-4 and the S100A8/S100A9 dimer have been shown to have significant responsibilities in irritant contact dermatitis and impaired hydration status, and TLR-4 is responsible for the production of TNF-α, IL-1β, and IL-6, proinflammatory cytokines through

MyD88 and NFKB pathways (Swanson et al., 2020; Vogl et al., 2014; Xu et al, 2014). TLR-4 is activated by lipopolysaccharides in bacterial cell walls, however, novel research has shown that TLR-4 can initiate changes in keratinocyte proliferation and migration without external stimuli (Lotzava-Weiss et al., 2017). Lotzava-Weiss et al. used a TLR-4 knockout HaCaT cell line to demonstrate that underexpression of this receptor can promote proliferation in keratinocytes, and overexpression can support migration in a scratch assay (2017). Knockout mice in this study also exhibited downregulation of IL-1β and IL-6 production at a nonhealing wound site, which supports the conclusion that activation of this receptor is important for healing wounds (Chen et al., 2013). In the present study, *TLR-4* expression was downregulated in 16 hour exposures for all photodegradation treatments while migration capabilities steadily increased with photodegradation length. Additionally, *IL-1β* was increasingly expressed as photodegradation time increased, and *IL-6* was downregulated in all treatment groups. This suggests that photodegraded treatments can bypass *TLR-4* signaling to produce sustained levels of *IL-1α* and *IL-1β*, but not *IL-6*.

Aryl hydrocarbon receptor (AhR) is an increasingly studied receptor for the intracellular processing of hydrocarbons (Noakes, 2015). It is expressed in all cells of the epidermis, although it is more concentrated in apical keratinocytes (Esser et al., 2013). Normal activation of AhR is necessary for protection against transepidermal water loss by sustaining keratinocyte differentiation (Tauchi et al., 2005). However, constitutive activation in keratinocytes can produce an atopic dermatitis phenotype that is accompanied by lesions and itching (Haas et al., 2016). AhR is both stimulated by, and produces reactive oxygen species (ROS) (Sutter et al., 2020). Direct damage to keratinocytes may cause the overproduction of ROS, which may stimulate the AhR to become activated. The cell viability assay results in this study suggests that

longer photodegradation treatments may negatively impact viability, and an ROS assay should be used to understand if cell viability is related to cytotoxicity by ROS formation under exposure conditions. Additionally, our study was limited to 17 proinflammatory molecules associated with keratinocyte inflammation and did not include AhR or any associated downstream molecules. An investigation of AhR activation upon exposure to photodegraded anthracene may be warranted if ROS formation is found to have a significant effect on cell viability.

Cytokines are important for initiating and sustaining immune-signaling cascades and regulating the transition from hemostasis and inflammation to proliferation and remodeling (Landen et al., 2016). Our investigation focused on the following proinflammatory cytokines: IL-6, IL-8, TNF-α, MIF, IL-1α, and IL-1β. These molecules can influence the expression of one other during an inflammatory response in epidermal tissue. For example, TNF-α signals through the TNF receptor and NFKB signaling pathways to produce IL-6, IL-8, IL-1β, and COX-2 (Lee at al., 2013; Udommethaporn et al., 2016*).* TNF-α and IL-1β both independently regulate IL-8 in response to changes in hydration status which relates to skin barrier function (Xu et al., 2014).

IL-1α, IL-1β, and TNF-α are commonly cited as major cytokines in irritant contact dermatitis pathologies, and these cytokines coordinate with fibroblasts and Langerhans cells to orchestrate an inflammatory response (Lee et al., 2013). TNF-α can also participate directly in the inflammatory response by supporting lymphocyte adhesion to fibroblasts, endothelial cells, and keratinocytes, thereby recruiting and maintaining immune activation in the epidermis. (Kock et al., 1990). This cytokine is implicated in wound repair, and mice treated with anti-TNF-α displayed significant delays in wound healing compared to control when treated with full-thickness wounds (Ritsu et al., 2017). Although not significant, our study shows that the relative expression of *TNF-α* was downregulated by four out of five photodegraded treatments at 4 hour

exposures, and then upregulated after 16 hours across all treatment groups. This temporal change may indicate a delay in expression at the early exposure time that is recovered after 16 hours.

The well documented inflammation cascade suggests that we should expect *IL-6, IL-8, IL-1β* and *COX-2* upregulated, yet we only find an upregulation in *IL-1β* and *IL-8* expression, where expression of *IL-6* and *COX-2* was similar to control values for 16 hour treatments. *IL-6* supports the proliferation and migration of keratinocytes and is overexpressed in psoriasis patients (Grossman et al., 1989; Yoshizaki et al., 1990). *IL-6* signal transduction is also necessary for timely wound healing and is thought to involve STAT3 pathways and relationships with fibroblasts (Gallucci et al., 2004).

COX-2 is normally present in differentiated keratinocytes, and both the COX-2 gene expression results and the reduced cytokeratin 10 staining in photodegraded treatments supports the conclusion that photodegrade anthracene may influence keratinocyte differentiation (Leong, 1996). This dysregulation in differentiation is similar to psoriasis phenotypes in which basal cells proliferate without differentiating (Albanesi et al., 2018). Our results indicate that although *TNF-α* is being expressed above control levels, it is not stimulating the pathways that produce *IL-6* and *COX-2*.

Interestingly, *IL-8* production appears unimpaired, and normal expression of this cytokine in keratinocytes is associated with monocyte recruitment, and it can function as a chemoattractant for keratinocyte migration to the wound site (Jiang et al., 2012). Overexpression of *IL-8* has also been associated with faster migration. We found that anthracene and photodegraded treatments resulted in an upregulation of *IL-8* at both 4 and 16 hour exposures, although neither trend was significant. These results suggest that *IL-8* production is likely dominated by *IL-1β* cascades, whereas signaling through NFKB to produce *IL-6* is limited in

treated cells. Literature suggests that downregulated *IL-6* production may interfere with keratinocyte migration and proliferation. However, our migration results demonstrate an increased migration capacity in 4-hour and 8-hour photodegraded treatments which suggests that *IL-8* can possibly recuperate migration functions in the absence of *IL-6*. This hypothesis can be further validated with a IL-6 knockout model in HaCaT keratinocytes.

A major limitation of gene expression analysis in a single cell type is that it cannot account for the cross-talk between keratinocytes and other major inflammatory cells. This limitation may explain the lack of upregulation in *CCL2*, which is also produced by fibroblasts in response to keratinocyte-derived IL-1α and TNF-α (Lee et al., 2013). MMP1 production in fibroblasts can be induced by IL-6, IL-1β, and TNF-α, and the absence of fibroblasts co-culture from this cell culture study may also account for the downregulation of *MMP1* expression (Moon et al., 2002; Wong et al., 2001).

Mus musculus Studies

Photodegraded anthracene initiates extracellular matrix remodeling in mouse epidermis

In the study on the mouse model, a total of 16 proinflammatory genes were assessed on mouse keratinocytes following a two week exposure to anthracene and photodegraded anthracene treatments. Eight genes showed little to no detectable expression and were thus omitted from subsequent analysis. The remaining genes including *Il-1α, Il-1β, Tlr-4, Ccl4, S100a9, Tnf-α, Mif, Mmp1*, *Connexin43*, and *Prss8* were used for statistical analysis. *IL-1β*, *S100a9, Mmp1,* and *Connexin43* demonstrated trends between treatment group and gene expression (Figure 14).

Two notable trends emerged for genes related to extracellular matrix remodeling and structure. Upregulation in gene expression for *Il-1β*, and *Mmp1, S100a9* for 4, 8, and 24-hour

photodegraded treatments was observed, and there was a corresponding downregulation in *Connexin43* for the same treatments (Figure 14). As previously mentioned, *Il-1β* is a proinflammatory cytokine that can regulate lymphocyte recruitment directly and indirectly (Chen et al., 2013; Lee et al., 2013). *Mmp1* is a matrix metalloproteinase that is involved in degrading the extracellular matrix to enhance keratinocyte and lymphocyte movement (Dumin et al., 2001). Mmps can potentially modify the function of other cytokines, and their roles can be both stimulating and downregulating (Dumin et al., 2001). *Mmp1* and *Mmp3* can degrade *Il-1β*, although *Mmp3* and *Mmp9* have also been demonstrated to activate it (Ito et al., 1996; Jobin et al., 2019; Manicone et al., 2008). The presence of *Mmp1* upregulation in concert with *Il-1β* in our *Mus musculus* results suggests that these two proinflammatory cytokines may be working in concert to recruit lymphocytes and allow them to permeate inflamed tissue (Figure 15). Additionally, *Il-1β* can induce fibroblasts to produce *Mmp1*, and the presence of fibroblasts in our mouse study may also account for greater expression levels (Wong et al., 2001). *Connexin43* is a cell to cell junction protein that is commonly expressed in basal layer cells (Zhang et al., 2017). In acute skin injuries, *Connexin43* is downregulated to support extracellular matrix remodeling and keratinocyte migration and proliferation (Zhang et al., 2017). We found a downregulation in gene expression that was corroborated by a decreased presence under immunofluorescent staining for 4, 8, and 24-hour photodegraded anthracene treatments (Figure 13). These trends support our findings in cell studies and suggest that photodegraded anthracene initiates a more severe response in epidermal remodeling than un-photodegraded anthracene treatments (Figure 15).

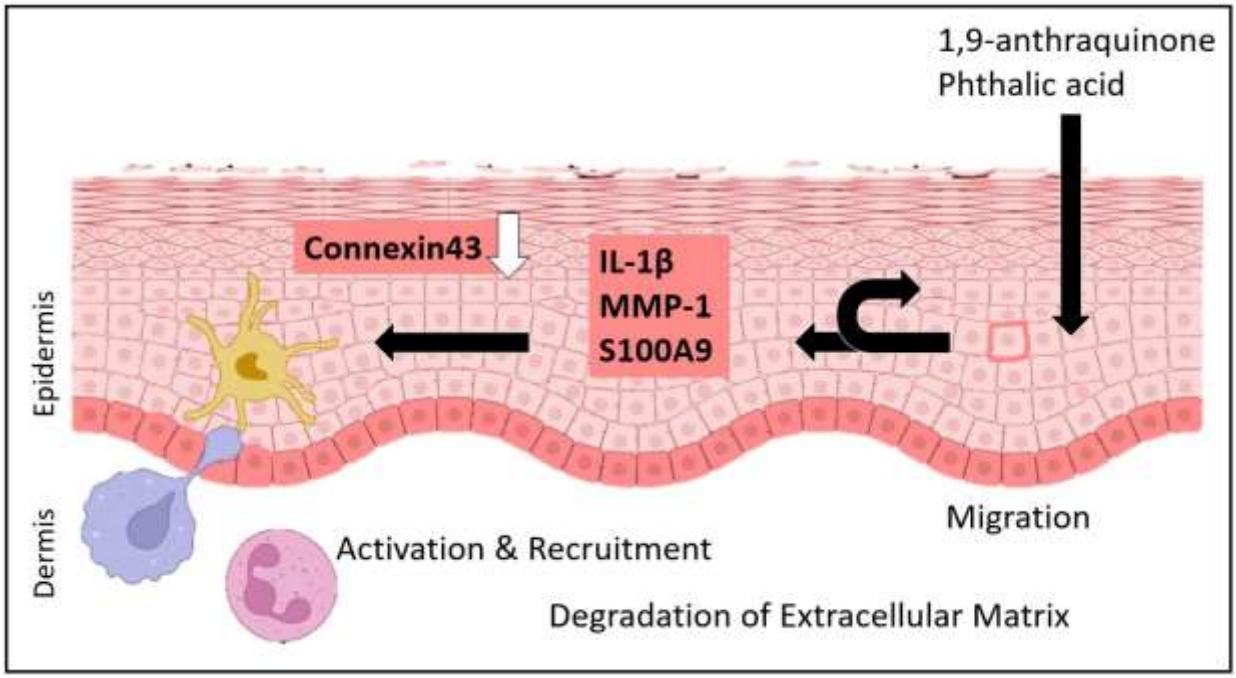

Figure 15: Proposed molecular mechanism of 1,9-anthraquinone and phthalic acid on keratinocytes in *Mus Musculus* epidermis. Image created on biorender.com.

S100a9 is an intracellular calcium-binding protein that has been used as a biomarker for ongoing inflammation in psoriasis patients (Kerkhoff et al., 2012). In the epidermis, *S100a9* can activate *Tlr-4* in macrophages when bound to *S100a8*, and thereby stimulate keratinocyte migration and decrease proliferation and survival (Christmann et al., 2021). Our findings of upregulated *S100a9* gene expression after exposure to 4, 8 and 24-hour photodegraded treatments are consistent with the effects on cell viability and migration capabilities observed in cell studies (Figure 4, Figure 5).

Gene expression patterns in *Mus musculus* are associated with the formation of the 9,10-anthraquinone and phthalic acid products in 8 and 24-hour photodegraded treatments. These results suggest that the intermediate products may be more potent irritants than anthracene in vivo, and these results should be further investigated with pure solutions of these intermediates.

Conclusion

Polycyclic aromatic hydrocarbons have been cited for their acute and chronic toxic effects on the skin, and their chemical modification under UV light makes them a priority group for study in dermal models. This study used both HaCaT keratinocytes in cell culture and isolated keratinocytes from mouse exposures to characterize the initiation of an inflammatory response to photodegraded anthracene. Photodegraded anthracene produced 1,9-anthraquinone and phthalic acid intermediates after 1 hour under simulated UV light. This study showed that cytotoxicity and activation of keratinocytes are enhanced with longer photodegradation treatments, and gene expression analysis suggests that these effects are mediated *by IL-1α, IL-1β*, and *TNF-α* but not *TLR-4*. An assessment of reactive oxygen species formation and AhR activation should be investigated to further understand if reactive oxygen species are involved in the keratinocyte response to photodegraded anthracene. Terminal differentiation of keratinocytes was also negatively affected by photodegradation treatments, but there were no differences in epidermal thickness for keratinocyte stratification or *Mus musculs* studies. *Il-1β* and *S100a9* were upregulated in both human keratinocyte and Mus musculus models, and functional analysis of these two genes is warranted to understand their importance in the keratinocyte inflammatory response. *Mus musculus* studies suggest that 4, 8, and 24-hour photodegraded anthracene can elicit extracellular matric remodeling that is associated with chronic inflammation, and future studies should confirm the isolated effects of 1,9-anthraquinone and phthalic acid exposure. These results provide a preliminary understanding of the harmful effects of photodegraded anthracene, and the quantification of these and other photodegraded PAH products should be prioritized in the environment.

REFERENCES

Abdel-Shafy, H. I., & Mansour, M. S. (2016). A review on polycyclic aromatic hydrocarbons: Source, environmental impact, effect on human health and remediation. *Egyptian Journal of Petroleum, 25*(1), 107-123. doi:10.1016/j.ejpe.2015.03.011

Alalaiwe, A., Lin, Y., Lin, C., Wang, P., Lin, J., & Fang, J. (2020). The absorption of polycyclic aromatic hydrocarbons into the skin to elicit cutaneous inflammation: The establishment of structure–permeation and in silico–in vitro–in vivo relationships. *Chemosphere, 255*, 126955. doi:10.1016/j.chemosphere.2020.126955

Albanesi, C., Madonna, S., Gisondi, P., & Girolomoni, G. (2018). The Interplay Between Keratinocytes and Immune Cells in the Pathogenesis of Psoriasis. *Frontiers in immunology*, *9*, 1549. https://doi.org/10.3389/fimmu.2018.01549

Avci, P., Sadasivam, M., Gupta, A., De Melo, W. C., Huang, Y. Y., Yin, R., Chandran, R., Kumar, R., Otufowora, A., Nyame, T., & Hamblin, M. R. (2013). Animal models of skin disease for drug discovery. *Expert opinion on drug discovery*, *8*(3), 331–355. https://doi.org/10.1517/17460441.2013.761202

Bacosa, H. P., Steichen, J., Kamalanathan, M., Windham, R., Lubguban, A., Labonté, J. M., . . . Quigg, A. (2020). Polycyclic aromatic hydrocarbons (PAHs) and putative PAH-degrading bacteria in Galveston Bay, TX (USA), following Hurricane Harvey (2017). *Environmental Science and Pollution Research, 27*(28), 34987-34999. doi:10.1007/s11356-020-09754-5

Bains, S. N., Nash, P., & Fonacier, L. (2018). Irritant contact dermatitis. *Clinical Reviews in Allergy & Immunology*, *56*(1), 99–109. https://doi.org/10.1007/s12016-018-8713-0

Bang, d., Lee, I. K., & Lee, B. M. (2011). Toxicological characterization of phthalic Acid. *Toxicological research*, *27*(4), 191–203. https://doi.org/10.5487/TR.2011.27.4.191

Behymer, T. D., & Hites, R. A. (1985). Photolysis of polycyclic aromatic hydrocarbons adsorbed on simulated atmospheric particulates. *Environmental Science & Technology*, *19*(10), 1004–1006. https://doi.org/10.1021/es00140a020

Benavides, F., Oberyszyn, T. M., VanBuskirk, A. M., Reeve, V. E., & Kusewitt, D. F. (2009). The hairless mouse in skin research. *Journal of dermatological science*, *53*(1), 10–18. https://doi.org/10.1016/j.jdermsci.2008.08.012

Blumer, M., & Youngblood, W. W. (1975). Polycyclic aromatic hydrocarbons in soils and recent sediments. *Science*, *188*(4183), 53–55. https://doi.org/10.1126/science.188.4183.53.

Centers for Disease Control and Prevention. (2013). *Polycyclic aromatic hydrocarbons (pahs): What health effects are associated with PAH exposure?* Centers for Disease Control and Prevention. Retrieved October 31, 2021, from https://www.atsdr.cdc.gov/csem/polycyclic-aromatic-hydrocarbons/health_effects.html#:~:text=Top%20of%20Page-,PAHs%20generally%20have%20a%20low%20degree%20of%20acute%20toxicity%20to,with%20occupational%20exposure%20to%20PAHs.

Clayton, K., Vallejo, A. F., Davies, J., Sirvent, S., & Polak, M. E. (2017). Langerhans cells—programmed by the epidermis. *Frontiers in Immunology*, *8*. https://doi.org/10.3389/fimmu.2017.01676

Chen, L., Guo, S., Ranzer, M. J., & DiPietro, L. A. (2013). Toll-like receptor 4 has an essential role in early skin wound healing. *Journal of Investigative Dermatology*, *133*(1), 258–267. https://doi.org/10.1038/jid.2012.267

Christmann, C., Zenker, S., Martens, L., Hübner, J., Loser, K., Vogl, T., & Roth, J. (2021). Interleukin 17 promotes expression of alarmins S100A8 and S100A9 during the inflammatory response of keratinocytes. *Frontiers in Immunology*, *11*. https://doi.org/10.3389/fimmu.2020.599947

Dąbrowska, D., Kot-Wasik, A., & Namieśnik, J. (2008). Stability studies of selected polycyclic aromatic hydrocarbons in different organic solvents and identification of their transformation products. *Polish Journal of Environmental Studies*, *17*(1).

Dover, R., & Potten, C. S. (1988). Heterogeneity and cell cycle analyses from time-lapse studies of human keratinocytes in vitro. *Journal of Cell Science*, *89*(3), 359–364. https://doi.org/10.1242/jcs.89.3.359

Dumin, J. A., Dickeson, S. K., Stricker, T. P., Bhattacharyya-Pakrasi, M., Roby, J. D., Santoro, S. A., & Parks, W. C. (2001). Pro-collagenase-1 (matrix metalloproteinase-1) binds the α2β1 integrin upon release from keratinocytes migrating on type I collagen. *Journal of Biological Chemistry*, *276*(31), 29368–29374. https://doi.org/10.1074/jbc.m104179200

Esser, C., Bargen, I., Weighardt, H., Haarmann-Stemmann, T., & Krutmann, J. (2013). Functions of the aryl hydrocarbon receptor in the skin. *Seminars in Immunopathology*, *35*(6), 677–691. https://doi.org/10.1007/s00281-013-0394-4

Fasnacht, M. P., & Blough, N. V. (2002). Aqueous photodegradation of polycyclic aromatic hydrocarbons. *Environmental Science & Technology*, *36*(20), 4364–4369. https://doi.org/10.1021/es025603k

Fu, P. P., Xia, Q., Sun, X., & Yu, H. (2012). Phototoxicity and environmental transformation of polycyclic aromatic hydrocarbons (pahs)—light-induced reactive oxygen species, lipid

peroxidation, and DNA damage. *Journal of Environmental Science and Health, Part C*, *30*(1), 1–41. https://doi.org/10.1080/10590501.2012.653887

Gallucci, R. M., Sloan, D. K., Heck, J. M., Murray, A. R., & O'Dell, S. J. (2004). Interleukin 6 indirectly induces keratinocyte migration. *Journal of Investigative Dermatology*, *122*(3), 764–772. https://doi.org/10.1111/j.0022-202x.2004.22323.x

Gamble, L. R., & Jackson, G. (1989). *CONTAMINANTS INVESTIGATION OF THE ARANSAS BAY COMPLEX, TEXAS, 1985-1986* (pp. 24-32) (United States of American, US Fish and Wildlife Service Ecological Services). Corpus Christi, TX.

Geier, M. C., Chlebowski, A. C., Truong, L., Massey Simonich, S. L., Anderson, K. A., & Tanguay, R. L. (2018). Comparative developmental toxicity of a comprehensive suite of polycyclic aromatic hydrocarbons. *Archives of toxicology*, *92*(2), 571–586. https://doi.org/10.1007/s00204-017-2068-9

Götz, C., Pfeiffer, R., Tigges, J., Ruwiedel, K., Hübenthal, U., Merk, H. F., Krutmann, J., Edwards, R. J., Abel, J., Pease, C., Goebel, C., Hewitt, N., & Fritsche, E. (2012). Xenobiotic metabolism capacities of human skin in comparison with a 3D-epidermis model and keratinocyte-based cell culture as in vitro alternatives for chemical testing: phase II enzymes. *Experimental dermatology*, *21*(5), 364–369. https://doi.org/10.1111/j.1600-0625.2012.01478.x

Grossman, R. M., Krueger, J., Yourish, D., Granelli-Piperno, A., Murphy, D. P., May, L. T., Kupper, T. S., Sehgal, P. B., & Gottlieb, A. B. (1989). Interleukin 6 is expressed in high levels in psoriatic skin and stimulates proliferation of cultured human keratinocytes. *Proceedings of the National Academy of Sciences*, *86*(16), 6367–6371. https://doi.org/10.1073/pnas.86.16.6367

Gruys, E., Toussaint, M. J., Niewold, T. A., & Koopmans, S. J. (2005). Acute phase reaction and acute phase proteins. *Journal of Zhejiang University. Science. B*, *6*(11), 1045–1056. https://doi.org/10.1631/jzus.2005.B1045

Guo, Y., Redmond, C. J., Leacock, K. A., Brovkina, M. V., Ji, S., Jaskula-Ranga, V., & Coulombe, P. A. (2020). Keratin 14-dependent disulfides regulate epidermal homeostasis and barrier function via 14-3-3σ and YAP1. *ELife*, *9*. https://doi.org/10.7554/elife.53165

Haas, K., Weighardt, H., Deenen, R., Köhrer, K., Clausen, B., Zahner, S., Boukamp, P., Bloch, W., Krutmann, J., & Esser, C. (2016). Aryl hydrocarbon receptor in keratinocytes is essential for murine skin barrier integrity. *Journal of Investigative Dermatology*, *136*(11), 2260–2269. https://doi.org/10.1016/j.jid.2016.06.627

Hassan, S. S., El Azab, W. I., Ali, H. R., & Mansour, M. S. (2015). Green synthesis and characterization of zno nanoparticles for photocatalytic degradation of anthracene. *Advances in Natural Sciences: Nanoscience and Nanotechnology*, *6*(4), 045012. https://doi.org/10.1088/2043-6262/6/4/045012

Hayakawa, K., Nomura, M., Nakagawa, T., Oguri, S., Kawanishi, T., Toriba, A., . . . Tamiya, E. (2006, March). Damage to and recovery of coastlines polluted with C-heavy oil spilled from the Nakhodka. *Water Research, 40*(5), 981-989. doi:10.1016/j.watres.2005.12.035

Hoffman, D. J. (2003). Petroleum and Individual Polycyclic Aromatic Hydrocarbons. In *Handbook of ecotoxicology* (pp. 348-350). London: Lewis. doi:https://doi.org/10.1201/9781420032505

Honda, M., & Suzuki, N. (2020). Toxicities of Polycyclic Aromatic Hydrocarbons for Aquatic Animals. *International journal of environmental research and public health*, *17*(4), 1363. https://doi.org/10.3390/ijerph17041363

Huang, X. D., Dixon, D. G., & Greenberg, B. M. (1995). Increased polycyclic aromatic hydrocarbon toxicity following their photomodification in natural sunlight: Impacts on the duckweed Lemna Gibba L. G-3. *Ecotoxicology and Environmental Safety*, *32*(2), 194–200. https://doi.org/10.1006/eesa.1995.1102

Jameson CW. Polycyclic aromatic hydrocarbons and associated occupational exposures. In: Baan RA, Stewart BW, Straif K, editors. Tumour Site Concordance and Mechanisms of Carcinogenesis. Lyon (FR): International Agency for Research on Cancer; 2019. (IARC Scientific Publications, No. 165.) Chapter 7. Available from: https://www.ncbi.nlm.nih.gov/books/NBK570325/

Juráňová, J., Franková, J., & Ulrichová, J. (2017). The role of keratinocytes in inflammation. *Journal of Applied Biomedicine*, *15*(3), 169–179. https://doi.org/10.1016/j.jab.2017.05.003

Kerkhoff, C., Voss, A., Scholzen, T. E., Averill, M. M., Zänker, K. S., & Bornfeldt, K. E. (2012). Novel insights into the role of S100A8/A9 in skin biology. *Experimental dermatology*, *21*(11), 822–826. https://doi.org/10.1111/j.1600-0625.2012.01571.x

Kim, D., Young, T. M., & Anastasio, C. (2013). Phototransformation rate constants of PAHs associated with soot particles. *The Science of the total environment*, *443*, 896–903. https://doi.org/10.1016/j.scitotenv.2012.11.055

Klicznik, M. M., Szenes-Nagy, A. B., Campbell, D. J., & Gratz, I. K. (2018). Taking the lead - how keratinocytes orchestrate skin T cell immunity. *Immunology letters*, *200*, 43–51. https://doi.org/10.1016/j.imlet.2018.06.009

Köck, A., Schwarz, T., Kirnbauer, R., Urbanski, A., Perry, P., Ansel, J. C., & Luger, T. A. (1990). Human keratinocytes are a source for tumor necrosis factor alpha: Evidence for

synthesis and release upon stimulation with endotoxin or ultraviolet light. *Journal of Experimental Medicine*, *172*(6), 1609–1614. https://doi.org/10.1084/jem.172.6.1609

Landén, N. X., Li, D., & Ståhle, M. (2016). Transition from inflammation to proliferation: a critical step during wound healing. *Cellular and molecular life sciences : CMLS*, *73*(20), 3861–3885. https://doi.org/10.1007/s00018-016-2268-0

Lee, H. Y., Stieger, M., Yawalkar, N., & Kakeda, M. (2013). Cytokines and chemokines in irritant contact dermatitis. *Mediators of inflammation*, *2013*, 916497. https://doi.org/10.1155/2013/916497

Leonard, A., & Guttman-Yassky, E. (2018). The unique molecular signatures of contact dermatitis and implications for treatment. *Clinical Reviews in Allergy & Immunology*, *56*(1), 1–8. https://doi.org/10.1007/s12016-018-8685-0

Leong, J., Hughes-Fulford, M., Rakhlin, N., Habib, A., Maclouf, J., & Goldyne, M. E. (1996). Cyclooxygenases in human and mouse skin and cultured human keratinocytes: association of COX-2 expression with human keratinocyte differentiation. *Experimental cell research*, *224*(1), 79–87. https://doi.org/10.1006/excr.1996.0113

Liang, C. C., Park, A. Y., & Guan, J. L. (2007). In vitro scratch assay: a convenient and inexpensive method for analysis of cell migration in vitro. *Nature protocols*, *2*(2), 329–333. https://doi.org/10.1038/nprot.2007.30

Liu, Z., Liu, J., & Wang, Z. (2011, October 19). The distribution of polycyclic aromatic hydrocarbons in surface sediments within the Mission-Aransas National Estuarine Research Reserve, Texas. Retrieved from https://utmsi.utexas.edu/images/MSI/NERR_report_Liu_10-19-2011.pdf

Lu, X. Y., Zhang, T., & Fang, H. H. (2011). Bacteria-mediated PAH degradation in soil and sediment. *Applied microbiology and biotechnology*, *89*(5), 1357–1371. https://doi.org/10.1007/s00253-010-3072-7

López-García, J., Lehocký, M., Humpolíček, P., & Sáha, P. (2014). HaCaT Keratinocytes Response on Antimicrobial Atelocollagen Substrates: Extent of Cytotoxicity, Cell Viability and Proliferation. *Journal of functional biomaterials*, *5*(2), 43–57. https://doi.org/10.3390/jfb5020043

Łyszczarz, S., Lasota, J., Szuszkiewicz, M. M., & Błońska, E. (2021). Soil texture as a key driver of polycyclic aromatic hydrocarbons (pahs) distribution in Forest Topsoils. *Scientific Reports*, *11*(1). https://doi.org/10.1038/s41598-021-94299-x

Malakahmad, A., Law, M. X., Ng, K.-W., & Manan, T. S. (2016). The fate and toxicity assessment of polycyclic aromatic hydrocarbons (pahs) in water streams of Malaysia. *Procedia Engineering*, *148*, 806–811. https://doi.org/10.1016/j.proeng.2016.06.572

Marquès, M., Mari, M., Audí-Miró, C., Sierra, J., Soler, A., Nadal, M., & Domingo, J. L. (2016). Photodegradation of polycyclic aromatic hydrocarbons in soils under a climate change base scenario. *Chemosphere*, *148*, 495–503. https://doi.org/10.1016/j.chemosphere.2016.01.069

Moorthy, B., Chu, C., & Carlin, D. J. (2015). Polycyclic aromatic hydrocarbons: from metabolism to lung cancer. *Toxicological sciences : an official journal of the Society of Toxicology*, *145*(1), 5–15. https://doi.org/10.1093/toxsci/kfv040

Moon, S. E., Bhagavathula, N., & Varani, J. (2002). Keratinocyte stimulation of matrix metalloproteinase-1 production and proliferation in fibroblasts: regulation through mitogen-activated protein kinase signalling events. *British journal of cancer*, *87*(4), 457–464. https://doi.org/10.1038/sj.bjc.6600478

National Center for Biotechnology Information (2021). PubChem Compound Summary for CID 8418, Anthracene. Retrieved December 11, 2021 from https://pubchem.ncbi.nlm.nih.gov/compound/Anthracene.

Natsuga K. (2014). Epidermal barriers. *Cold Spring Harbor perspectives in medicine*, *4*(4), a018218. https://doi.org/10.1101/cshperspect.a018218

Noakes R. (2015). The aryl hydrocarbon receptor: a review of its role in the physiology and pathology of the integument and its relationship to the tryptophan metabolism. *International journal of tryptophan research : IJTR*, *8*, 7–18. https://doi.org/10.4137/IJTR.S19985

Parrado, C., Mercado-Saenz, S., Perez-Davo, A., Gilaberte, Y., Gonzalez, S., & Juarranz, A. (2019). Environmental stressors on skin aging. mechanistic insights. *Frontiers in Pharmacology*, *10*. https://doi.org/10.3389/fphar.2019.00759

Pasparakis, M., Haase, I., & Nestle, F. O. (2014). Mechanisms regulating skin immunity and inflammation. *Nature Reviews Immunology*, *14*(5), 289–301. https://doi.org/10.1038/nri3646

Patel, A. B., Shaikh, S., Jain, K. R., Desai, C., & Madamwar, D. (2020). Polycyclic aromatic hydrocarbons: Sources, toxicity, and remediation approaches. *Frontiers in Microbiology*, *11*. https://doi.org/10.3389/fmicb.2020.562813

Pelletier, M. C., Burgess, R. M., Ho, K. T., Kuhn, A., McKinney, R. A., & Ryba, S. A. (1997). Phototoxicity of individual polycyclic aromatic hydrocarbons and petroleum to marine invertebrate larvae and juveniles. *Environmental Toxicology and Chemistry*, *16*(10), 2190–2199. https://doi.org/10.1002/etc.5620161029

Polycyclic aromatic hydrocarbons (pahs) fact sheet. US EPA. (n.d.). Retrieved November 3, 2021, from https://19january2021snapshot.epa.gov/sites/static/files/2014-03/documents/pahs_factsheet_cdc_2013.pdf.

Raj, D., Brash, D. E., & Grossman, D. (2006). Keratinocyte apoptosis in epidermal development and disease. *The Journal of investigative dermatology*, *126*(2), 243–257. https://doi.org/10.1038/sj.jid.5700008

Rengarajan, T., Rajendran, P., Nandakumar, N., Lokeshkumar, B., Rajendran, P., & Nishigaki, I. (2015). Exposure to polycyclic aromatic hydrocarbons with special focus on cancer. *Asian Pacific Journal of Tropical Biomedicine*, *5*(3), 182–189. https://doi.org/10.1016/s2221-1691(15)30003-4

Ritsu, M., Kawakami, K., Kanno, E., Tanno, H., Ishii, K., Imai, Y., Maruyama, R., & Tachi, M. (2017). Critical role of tumor necrosis factor-α in the early process of wound healing in skin. *Journal of Dermatology & Dermatologic Surgery*, *21*(1), 14–19. https://doi.org/10.1016/j.jdds.2016.09.001

Rodrigues, M., Kosaric, N., Bonham, C. A., & Gurtner, G. C. (2019). Wound healing: A cellular perspective. *Physiological Reviews*, *99*(1), 665–706. https://doi.org/10.1152/physrev.00067.2017

Ronfard, V., & Barrandon, Y. (2001, April 10). *Migration of keratinocytes through tunnels of digested fibrin*. Proceedings of the National Academy of Sciences of the United States of America. Retrieved November 2, 2021, from https://www.ncbi.nlm.nih.gov/sites/ppmc/articles/PMC31864/.

Roshan, A., Murai, K., Fowler, J., Simons, B. D., Nikolaidou-Neokosmidou, V., & Jones, P. H. (2016). Human keratinocytes have two interconvertible modes of proliferation. *Nature cell biology*, *18*(2), 145–156. https://doi.org/10.1038/ncb3282.

Rosso, J. D., Zeichner, J., Alexis, A., Cohen, D., & Berson, D. (2016). Understanding the Epidermal Barrier in Healthy and Compromised Skin: Clinically Relevant Information for the Dermatology Practitioner: Proceedings of an Expert Panel Roundtable Meeting. *The Journal of clinical and aesthetic dermatology*, *9*(4 Suppl 1), S2–S8.

Rowe, G. T., Fernando, H., Elferink, C., Ansari, G., Sullivan, J., Heathman, T., Quigg, A., Petronella Croisant, S., Wade, T. L., & Santschi, P. H. (2020). Polycyclic aromatic hydrocarbons (PAHs) cycling and fates in Galveston Bay, Texas, USA. *PloS one*, *15*(12), e0243734. https://doi.org/10.1371/journal.pone.0243734

Seopela, M. P., Powers, L. C., Clark, C., Heyes, A., & Gonsior, M. (2021). Combined fluorescent measurements, parallel factor analysis and GC-mass spectrometry in evaluating the photodegradation of PAHS in freshwater systems. *Chemosphere*, *269*, 129386. https://doi.org/10.1016/j.chemosphere.2020.129386

Slodownik, D., Lee, A., & Nixon, R. (2008). Irritant contact dermatitis: A Review. *Australasian Journal of Dermatology*, *49*(1), 1–11. https://doi.org/10.1111/j.1440-0960.2007.00409.x

Sowada, J., Lemoine, L., Schön, K., Hutzler, C., Luch, A., & Tralau, T. (2017). Toxification of polycyclic aromatic hydrocarbons by commensal bacteria from human skin. *Archives of Toxicology*, *91*(6), 2331–2341. https://doi.org/10.1007/s00204-017-1964-3

Stec, A. A., Dickens, K. E., Salden, M., Hewitt, F. E., Watts, D. P., Houldsworth, P. E., & Martin, F. L. (2018). Occupational exposure to polycyclic aromatic hydrocarbons and

elevated cancer incidence in firefighters. *Scientific Reports*, *8*(1). https://doi.org/10.1038/s41598-018-20616-6

St. Michael's Hospital Research (n.d.). *Hematoxylin and Eosin Staining - Manual protocol*.. Retrieved May 7, 2022, Adapted from Baylor College of Medicine. from http://stmichaelshospitalresearch.ca/wp-content/uploads/2017/05/Hematoxylin-and-Eosin-HE-Staining-%E2%80%93-Manual-Protocol.pdf

Sutter, C. H., Rainwater, H. M., & Sutter, T. R. (2020). Contributions of nitric oxide to ahr-ligand-mediated keratinocyte differentiation. *International Journal of Molecular Sciences*, *21*(16), 5680. https://doi.org/10.3390/ijms21165680

Swanson, L., Katkar, G. D., Tam, J., Pranadinata, R. F., Chareddy, Y., Coates, J., Anandachar, M. S., Castillo, V., Olson, J., Nizet, V., Kufareva, I., Das, S., & Ghosh, P. (2020). TLR4 signaling and macrophage inflammatory responses are dampened by Giv/Girdin. *Proceedings of the National Academy of Sciences*, *117*(43), 26895–26906. https://doi.org/10.1073/pnas.2011667117

Tauchi, M., Hida, A., Negishi, T., Katsuoka, F., Noda, S., Mimura, J., Hosoya, T., Yanaka, A., Aburatani, H., Fujii-Kuriyama, Y., Motohashi, H., & Yamamoto, M. (2005). Constitutive expression of aryl hydrocarbon receptor in keratinocytes causes inflammatory skin lesions. *Molecular and cellular biology*, *25*(21), 9360–9368. https://doi.org/10.1128/MCB.25.21.9360-9368.2005

Udommethaporn, S., Tencomnao, T., McGowan, E. M., & Boonyaratanakornkit, V. (2016). Assessment of Anti-TNF-α Activities in Keratinocytes Expressing Inducible TNF- α: A Novel Tool for Anti-TNF-α Drug Screening. *PloS one*, *11*(7), e0159151. https://doi.org/10.1371/journal.pone.0159151

van den Bogaard, E. H., Podolsky, M. A., Smits, J. P., Cui, X., John, C., Gowda, K., Desai, D., Amin, S. G., Schalkwijk, J., Perdew, G. H., & Glick, A. B. (2015). Genetic and pharmacological analysis identifies a physiological role for the AHR in epidermal differentiation. *The Journal of investigative dermatology*, *135*(5), 1320–1328. https://doi.org/10.1038/jid.2015.6

Vogl, T., Eisenblätter, M., Völler, T., Zenker, S., Hermann, S., van Lent, P., Faust, A., Geyer, C., Petersen, B., Roebrock, K., Schäfers, M., Bremer, C., & Roth, J. (2014). Alarmin S100A8/S100A9 as a biomarker for molecular imaging of local inflammatory activity. *Nature Communications*, *5*(1). https://doi.org/10.1038/ncomms5593

Wang, S., Sheng, Y., Feng, M., Leszczynski, J., Wang, L., Tachikawa, H., & Yu, H. (2007). Light-induced cytotoxicity of 16 polycyclic aromatic hydrocarbons on the US EPA priority pollutant list in human skin HaCaT keratinocytes: relationship between phototoxicity and excited state properties. *Environmental toxicology*, *22*(3), 318–327. https://doi.org/10.1002/tox.20241

Wang, F., Zieman, A., & Coulombe, P. A. (2016). Skin Keratins. *Methods in enzymology*, *568*, 303–350. https://doi.org/10.1016/bs.mie.2015.09.032

Wong WR, Kossodo S, Kochevar IE. Influence of cytokines on matrix metalloproteinases produced by fibroblasts cultured in monolayer and collagen gels. J Formos Med Assoc. 2001 Jun;100(6):377-82. PMID: 11480246.

Woodley, D. T., Wysong, A., DeClerck, B., Chen, M., & Li, W. (2015). Keratinocyte Migration and a Hypothetical New Role for Extracellular Heat Shock Protein 90 Alpha in Orchestrating Skin Wound Healing. *Advances in wound care*, *4*(4), 203–212. https://doi.org/10.1089/wound.2014.0566

Xiao, T., Yan, Z., Xiao, S. *et al.* Proinflammatory cytokines regulate epidermal stem cells in wound epithelialization. *Stem Cell Res Ther* **11,** 232 (2020). https://doi.org/10.1186/s13287-020-01755-y

Xu, W., Jia, S., Xie, P., Zhong, A., Galiano, R. D., Mustoe, T. A., & Hong, S. J. (2014). The expression of proinflammatory genes in epidermal keratinocytes is regulated by hydration status. *Journal of Investigative Dermatology*, *134*(4), 1044–1055. https://doi.org/10.1038/jid.2013.425

Xu W, Vebrosky EN, Armbrust KL. (2018). Potential risk to human skin cells from exposure to dicloran photodegradation products in water. Environ;121(Pt 1):861-870. doi: 10.1016/j.envint.2018.10.010. Epub 2018 Oct 18. PMID: 30343185

Yan, J., Wang, L., Fu, P. P., & Yu, H. (2004). Photomutagenicity of 16 polycyclic aromatic hydrocarbons from the US EPA priority pollutant list. *Mutation research, 557*(1), 99–108. https://doi.org/10.1016/j.mrgentox.2003.10.004

Yoshizaki, K., Nishimoto, N., Matsumoto, K., Tagoh, H., Taga, T., Deguchi, Y., Kuritani, T., Hirano, T., Hashimoto, K., & Okada, N. (1990). Interleukin 6 and expression of its receptor on epidermal keratinocytes. *Cytokine*, *2*(5), 381–387. https://doi.org/10.1016/1043-4666(90)90069-6

Yousef, H., Alhaj, M., & Sharma, S. (n.d.). Anatomy, Skin (Integument), Epidermis. In *NCBI*. essay. Retrieved December 7, 2021, from https://www.ncbi.nlm.nih.gov/books/NBK430685/.

Yu, Hongtao (2002) ENVIRONMENTAL CARCINOGENIC POLYCYCLIC AROMATIC HYDROCARBONS: PHOTOCHEMISTRY AND PHOTOTOXICITY, Journal of Environmental Science and Health, Part C, 20:2, 149-183, doi: 10.1081/GNC-120016203

Zanoni, T. B., Tiago, M., Faião-Flores, F., de Moraes Barros, S. B., Bast, A., Hageman, G., de Oliveira, D. P., & Maria-Engler, S. S. (2014). Basic red 51, a permitted semi-permanent hair dye, is cytotoxic to human skin cells: Studies in monolayer and 3D skin model using human keratinocytes (HaCaT). *Toxicology Letters*, *227*(2), 139–149. https://doi.org/10.1016/j.toxlet.2014.03.007

Zhang, X. F., & Cui, X. (2017). Connexin 43: Key roles in the skin. *Biomedical reports*, *6*(6), 605–611. https://doi.org/10.3892/br.2017.903

APPENDIX

ADJUSTED P VALUES FOR ONE-WAY ANOVA

	tlr4	***tnfa***	***mif***	***mmp1***	***il1b***	***il1a***	***ccl4l2***	***s100a9***	***s100a8***	***il8***	***il6***	***ccl2***	***cxcl2***	***cox2***	***mmp3***	***mmp9***	***connexin43***
4 Hour Exposure																	
Anth	0.9790	1.0000	1.0000	0.9998	1.0000	0.9944	0.7730	1.0000	1.0000	0.9990	0.9980	1.0000	1.0000	0.7750	0.8000	0.7060	0.9458
PD-1h	0.9970	0.8380	0.9850	1.0000	0.5260	0.1940	0.6420	0.9530	1.0000	0.9590	0.9480	1.0000	0.9870	0.9940	1.0000	0.9010	1.0000
PD-4h	0.7150	0.8320	1.0000	0.1290	0.3720	*0.0989*	1.0000	0.6280	**0.0442***	0.9810	0.3570	0.5820	0.5390	0.2280	1.0000	0.9880	0.9990
PD-8h	0.8180	0.1690	0.6290	0.9976	0.5930	0.7775	0.7160	0.3630	0.9734	0.4510	0.4030	1.0000	1.0000	0.9870	0.9250	0.9500	0.6912
PD-24h	0.5320	0.4460	0.8800	0.9994	0.9720	0.8927	0.2540	0.9990	1.0000	1.0000	1.0000	1.0000	1.0000	0.9960	0.7780	1.0000	0.5760
16 Hour Exposure																	
Anth	0.2621	0.5850	**0.0164***	0.2305	0.9930	1.0000	0.7554	0.6350	0.9870	0.8280	0.8820	0.9530	0.2644	0.3220	0.2340	1.0000	1.0000
PD-1h	0.1027	0.9060	**0.0200***	**0.0100***	0.6102	0.8590	0.1734	0.7930	1.0000	0.4250	0.9990	0.9420	0.1485	0.6260	0.2480	0.5631	1.0000
PD-4h	0.1274	0.4530	0.9998	0.0814	0.2043	0.2430	0.9998	0.8210	0.9610	0.7840	1.0000	0.9940	0.8568	1.0000	0.2460	0.9999	0.9920
PD-8h	0.4343	0.3720	**0.0474***	0.3123	*0.0996*	0.1530	0.9999	0.2060	0.9970	0.2530	1.0000	1.0000	*0.0584*	1.0000	0.5550	0.9984	0.5740
PD-24h	**0.00727****	0.6840	0.9201	0.7716	0.5162	0.5520	0.9962	0.9470	0.3680	0.4970	0.9990	1.0000	0.5509	0.9770	0.3330	0.4220	0.7430

Appendix A: Adjusted p values for multiple comparisons of gene expression between treatment and control for each gene for HaCaT keratinocytes exposed to anthracene and photodegraded anthracene treatments for 4 and 16 hours. *$0.01<p<0.05$; **$p<0.01$